**A**

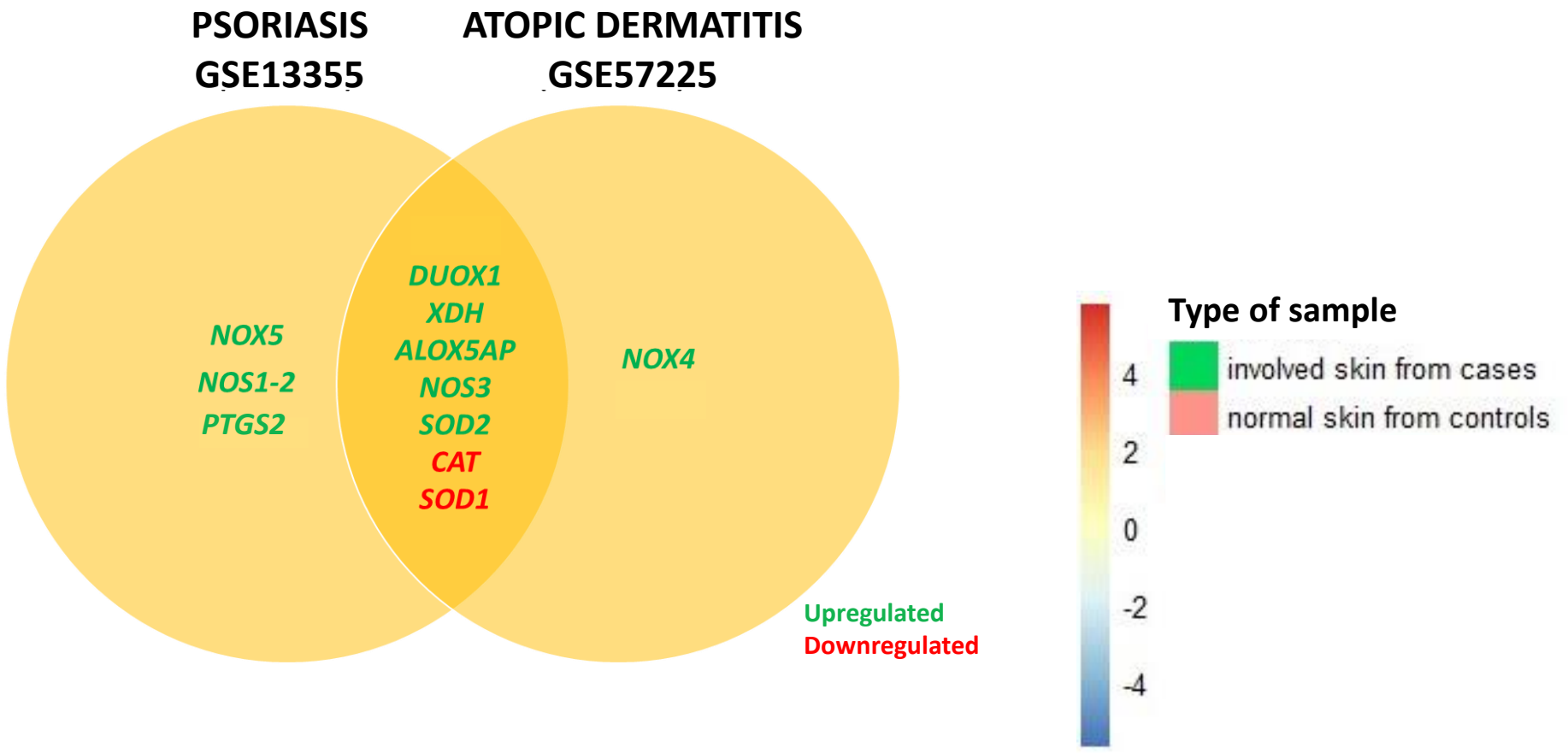


**B**

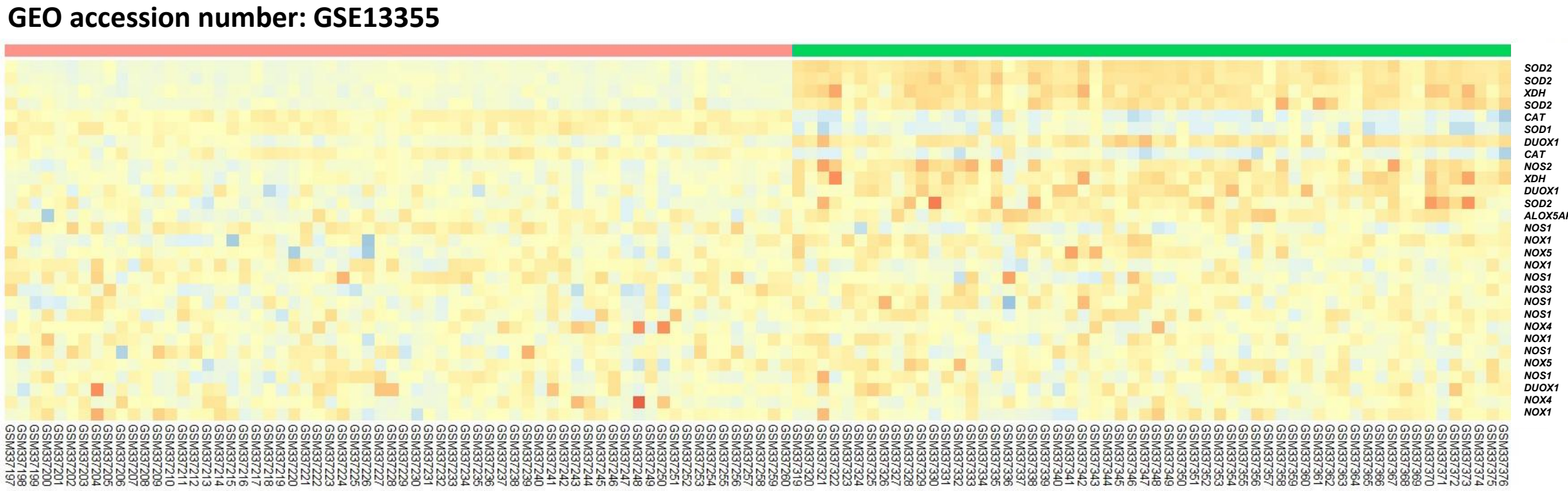


**C**

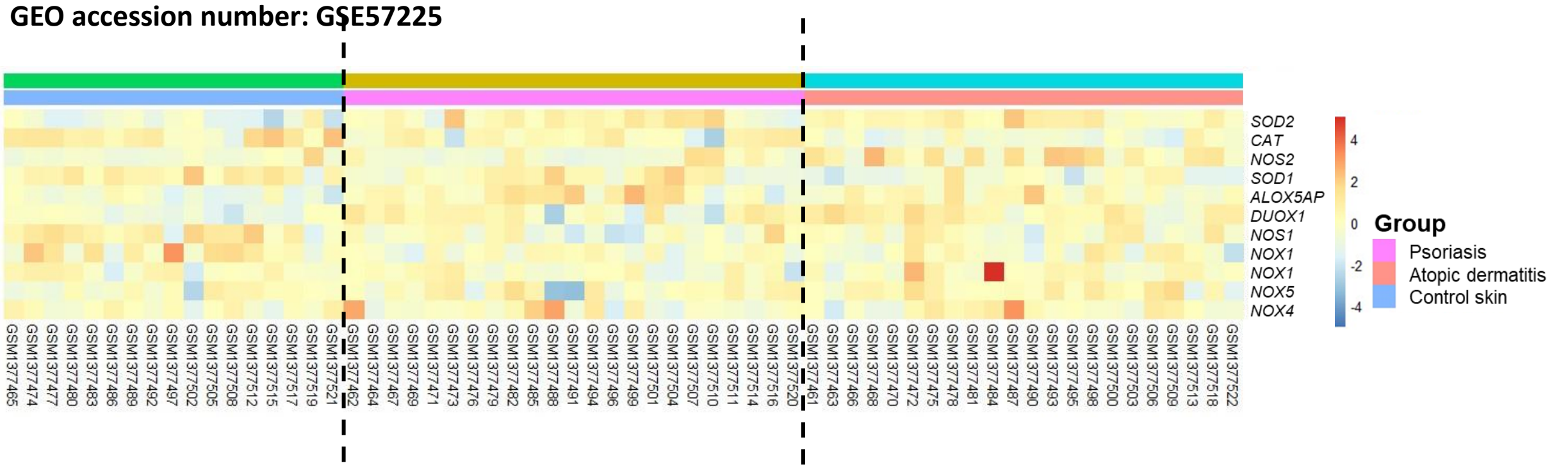


**Figure S1. Differential expression profiles of genes encoding key oxidative/nitrosative and antioxidant enzymes in psoriasis and atopic dermatitis.** Transcriptomic data from human psoriasis (GSE13355) and atopic dermatitis (GSE57225) samples from the Gene Expression Omnibus (GEO) database were analyzed. **(A)** Venn diagram showing common and specific gene transcript levels in each type of samples. **(B)** Heatmap showing gene transcript levels in psoriasis (GSE13355) samples versus control samples. **(C)** Heatmap showing analyzed transcript levels in atopic dermatitis (GSE57225) samples versus psoriasis and control samples. The heatmaps present duplicates or triplicates of the same gene because the data come from a microarray experiment containing different probes for the same gene.

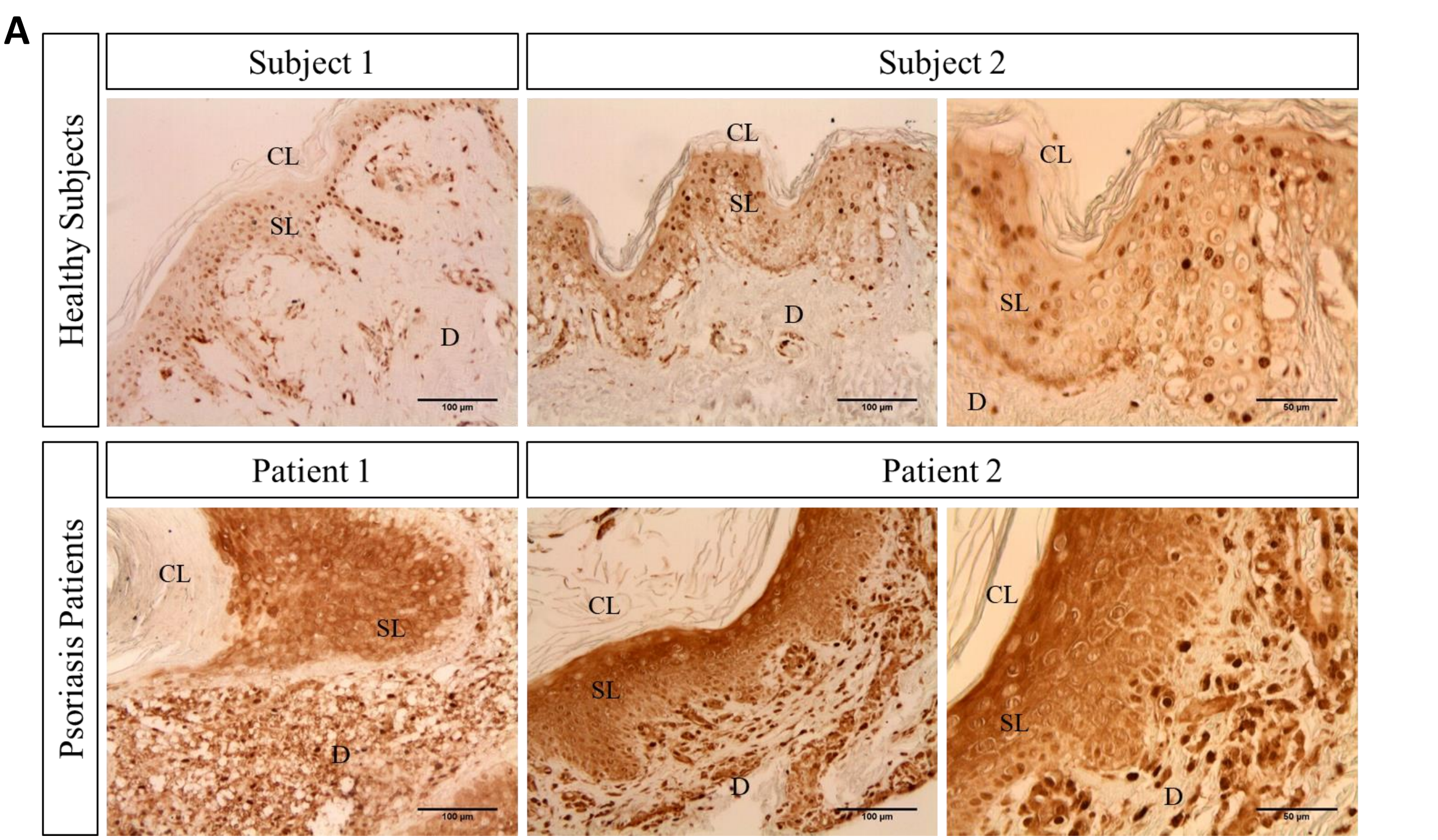


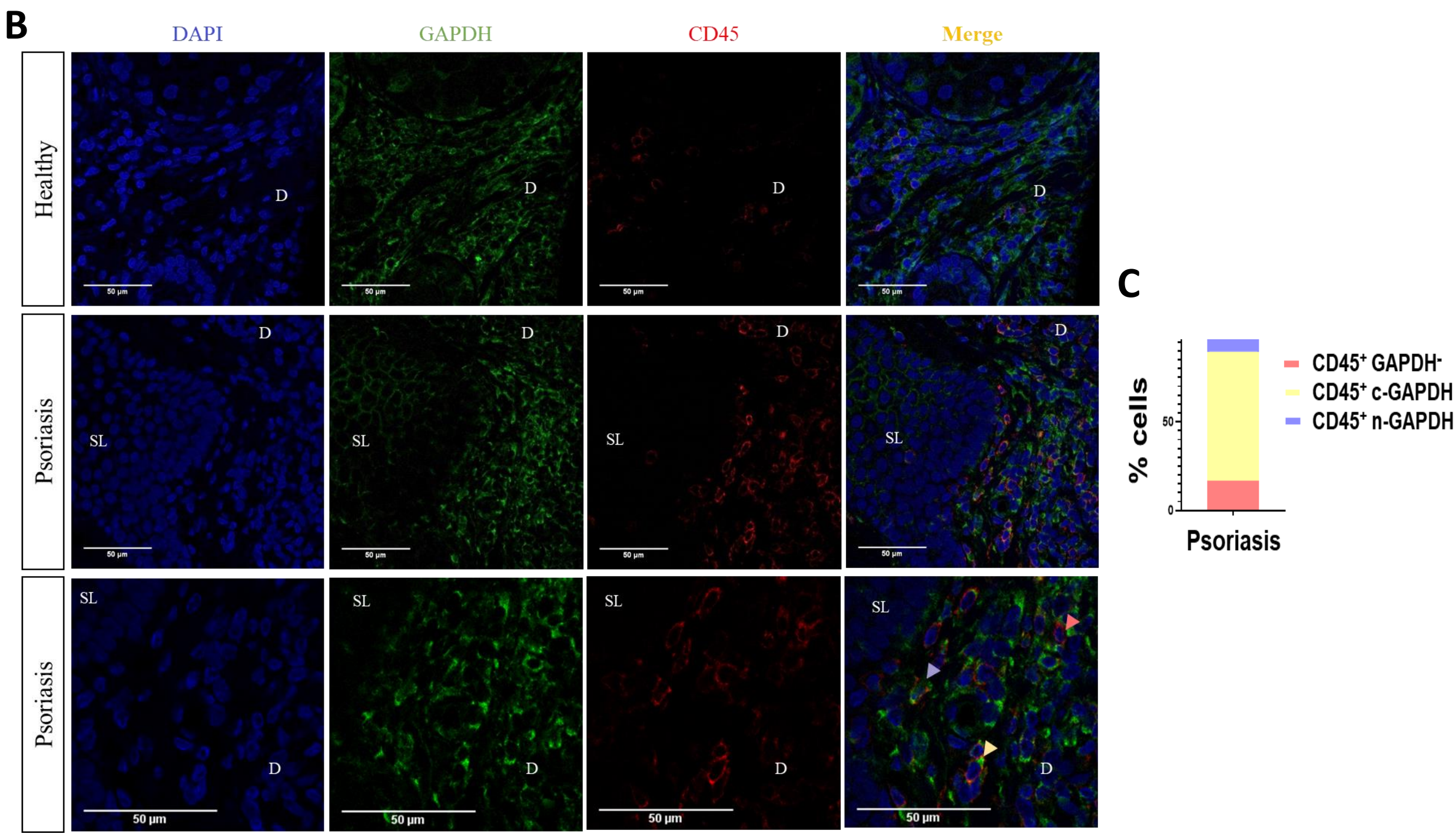


**Figure S2. Increased GAPDH levels and altered subcellular localization in the lesional skin of psoriasis patients. (A)** Representative images of skin biopsies from two healthy subjects and two psoriasis patients immunostained with anti-GAPDH. **(B, C)** Representative immunofluorescence images of skin sections from a healthy subject and a psoriasis patient stained with a rabbit anti-GAPDH (green) and a mouse anti-human CD45 antibody, counterstained with DAPI, and examined under a confocal microscope (Leica STELLARIS 8) and further processed with Leica software and ImageJ. The objective used was x63. B). Percentage of $CD45^+$ cells negative for GAPDH (red), with cytoplasmic GAPDH (c-GAPDH, yellow) and with nuclear GAPDH (n-GAPDH, violet) in skin sections from 3 psoriasis patients. Quantification was carried out by counting the number of cells of each type in three distinct regions from each of the three biopsies analyzed. After that, the abundance, in percentage, of each of these subset was calculated. CS, corneum layer; SS, spinosus layer; D, dermis; Bars: 50 µM.

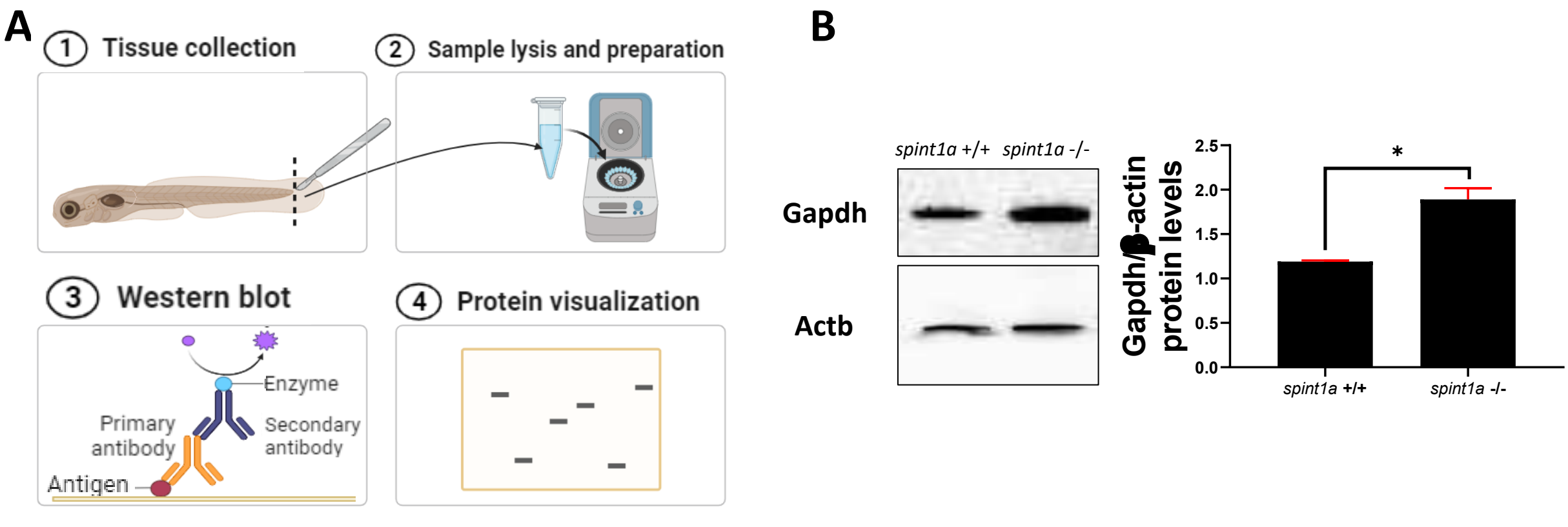


**Figure S3. Robust expression of nuclear Gapdh in the skin of Spint1a-deficient larvae. (A)** The final part of the tail of 72 hpf larvae was collected and the samples were then processed for western blot to determine Gapdh levels. **(B)** Gapdh and β-actin protein amounts in tail skin of wild type and Spint1a-deficient larvae treated. Results are shown as the mean ± SD for each group. p-Values were calculated using Student's *t* test. *p≤0.05. Gapdh, Glyceraldehyde 3-Phosphate Dehydrogenase; Actb, β-actin

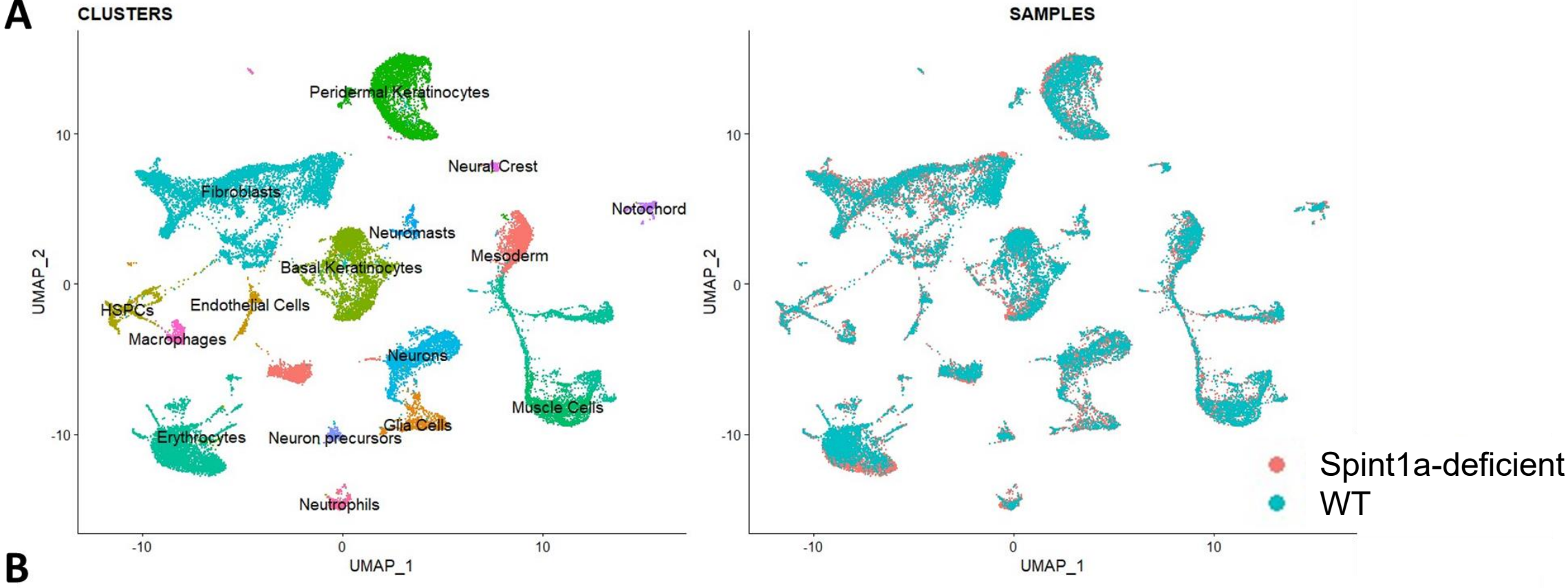


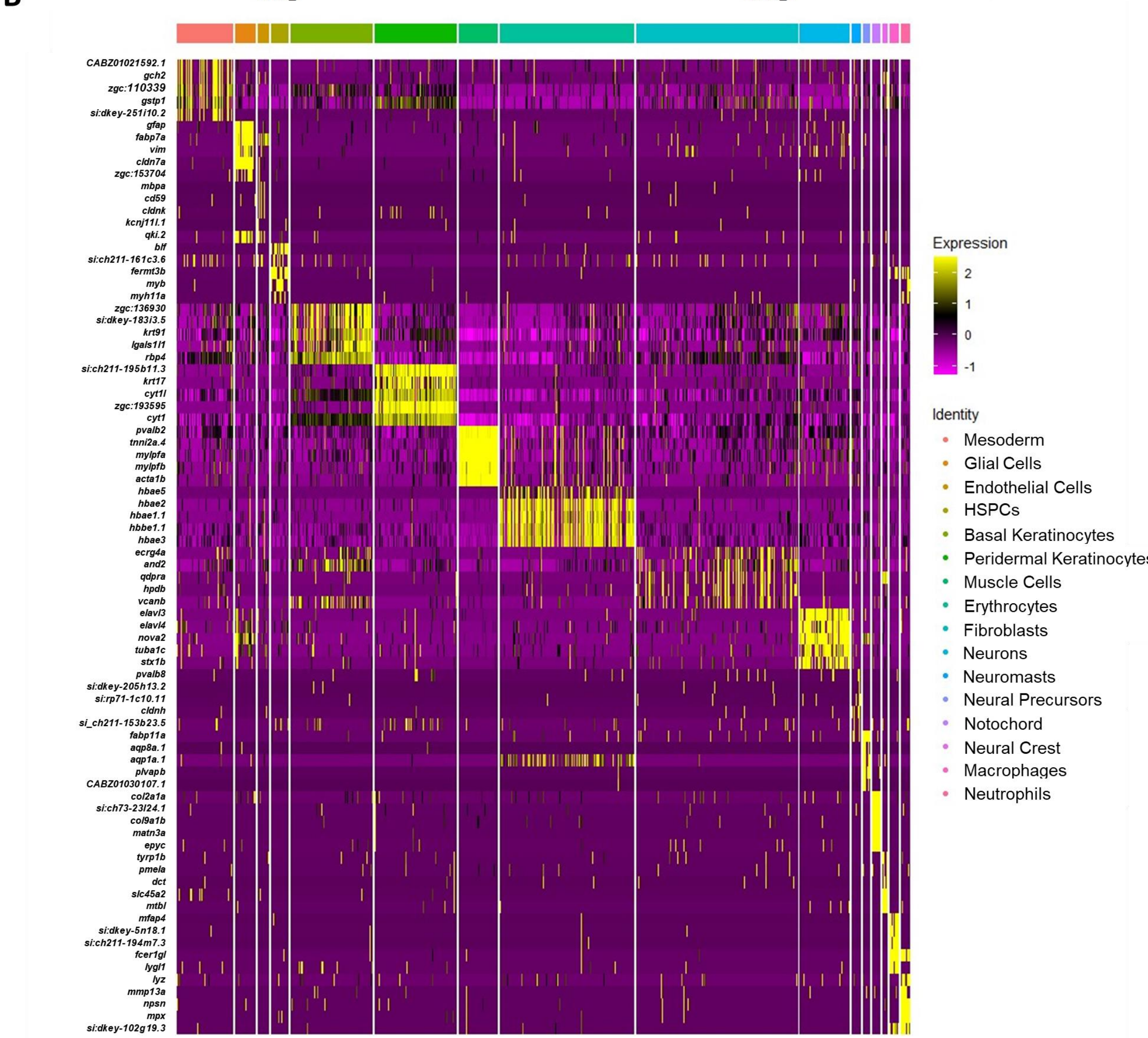


**Figure S4. Single cell RNA-seq of tails of wild type and Spint1a-deficient larvae reveals 17 different cell clusters. (A)** UMAP representation of the different cells analyzed by scRNA-seq pooled tails from 3 dpf larvae. Left, cluster annotation are shown in distinct colors. Right, cells are classified depending on the sample of origin: wild type (WT) or Spint1a-deficient larvae. **(B)** Heatmap showing the 5 most differentially expressed genes of each annotated cluster. The list was determined using Wilcoxon Rank Sum test to identify differentially expressed genes between groups. HSPCs, hematopoietic stem and progenitor cells; UMAP, Uniform Manifold Approximation.

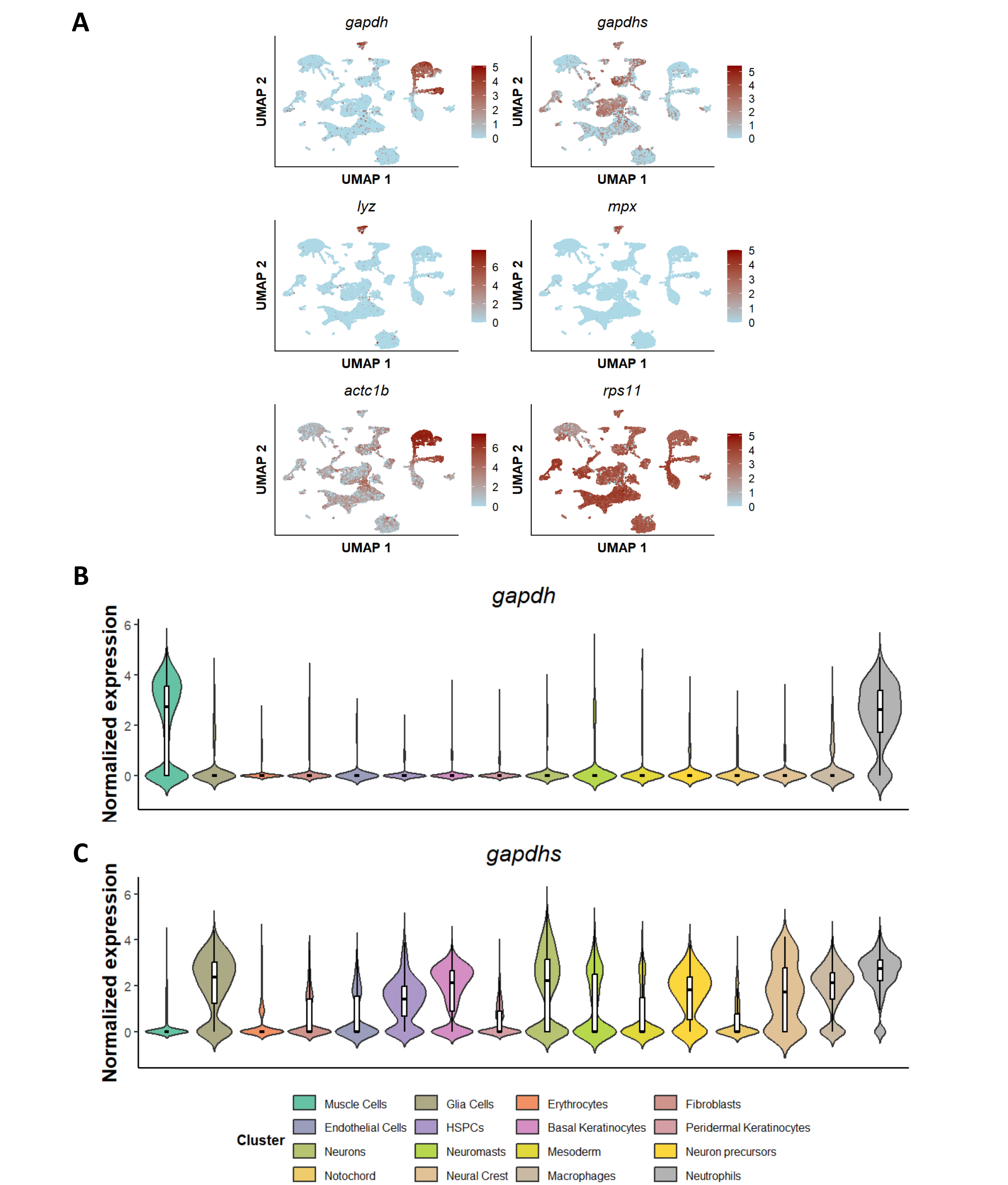


**Figure S5. Expression profile of *gapdh* and *gapdhs* in the different cell clusters. (A)** Single cell RNA-seq Feature Plot showed *gapdh* expression in muscle cell cluster (*actc1b*$^{+}$ cells) and neutrophils cluster (*mpx*$^{+}$ cells). The expression of *rps11* was used as a housekeeping gene. **(B, C)** Violin plots showing the expression of *gapdh* (B) and *gapdhs* (C) along the different clusters obtained. Each point represents the gene transcript levels in each cell analyzed.

```
Percent Identity  Matrix - created by Clustal2.1


  1: sp|Q5XJ10|G3P_DANRE   100.00   76.51
  2: sp|Q5MJ86|G3P2_DANRE   76.51  100.00
```

sp|Q5XJ10|G3P_DANRE 0.23494
sp|Q5MJ86|G3P2_DANRE 0.23494

```
sp|Q5XJ10|G3P_DANRE      --MVKVGINGFGRIGRLVTRAAFLTKKVEIVAINDPFIDLDYMVYMFQYDSTHGKYKGEV  58
sp|Q5MJ86|G3P2_DANRE     MSELCVGINGFGRIGRLVLRAC-LQKGIKVTAINDPFIDLQYMVYMFKYDSTHGRYKGEV  59
                            : ************ **. * * :::.*********:******:******:*****

sp|Q5XJ10|G3P_DANRE      KAEGGKLVIDGHAITVYSERDPANIKWGDAGATYVVESTGVFTTIEKASAHIKGGAKRVI  118
sp|Q5MJ86|G3P2_DANRE     HMEDGKLIVDGQAISVFQCMKPAEIPWGDAGALYVVESTGVFLSIEKASAHIQGGAKRVV  119
                         : *.***:**:**:*:.  .**:* ****** ********* :********:******:

sp|Q5XJ10|G3P_DANRE      ISAPSADAPMFVMGVNHEKYDN-SLTVVSNASCTTNCLAPLAKVINDNFVIVEGLMSTVH  177
sp|Q5MJ86|G3P2_DANRE     VSAPSPDAPMFVMGVNQDKYDPSSMTIVSNASCTTNCLAPLAKVIHDNFGIEEALMTTVH  179
                         :**** **********:***  *:*:******************:*** * *.**:***

sp|Q5XJ10|G3P_DANRE      AITATQKTVDGPSGKLWRDGRGASQNIIPASTGAAKAVGKVIPELNGKLTGMAFRVPTPN  237
sp|Q5MJ86|G3P2_DANRE     AYTATQKTVDGPSAKAWRDGRGAHQNIIPASTGAAKAVGKVIPELNGKLTGMAFRVPVAD  239
                         * **********.* ******* ********************************. :

sp|Q5XJ10|G3P_DANRE      VSVVDLTVRLEKPAKYDEIKKVVKAAADGPMKGILGYTEHQVVSTDFNGDCRSSIFDAGA  297
sp|Q5MJ86|G3P2_DANRE     VSVVDLTCRLTRPASYANIKESVKKAAHGPMKGILGYTEDSVVSSDFVGDTHSSIFDAGA  299
                         ******* ** :**.* :**: ** **.**********..***:** ** :********

sp|Q5XJ10|G3P_DANRE      GIALNDHFVKLVTWYDNEFGYSNRVCDLMAHMASKE  333
sp|Q5MJ86|G3P2_DANRE     GISLNDNFVKLISWYDNEFGYSHRVADLLMYMHSKE  335
                         **:***:****:*********:**.**: :* ***
```

**Figure S6. Protein sequence alignment of zebrafish Gapdh and Gapdhs.** Aligment using Clustal Omega showed a strong identity of 76,51% between both proteins, observed along all the sequence of the proteins, which showed also a similar number of amino-acids in their polypeptide chain, being 333 in the case of Gapdh and 335 in the case of Gapdhs. The conserved residue Cys-150 involved in nuclear translocation (corresponding to Cys-152 of human GAPDH) is highlighted in red. An asterisk (*) indicates positions which have a conserved residue; A colon (:) indicates conservation between groups of strongly similar properties. (.) indicates conservation between groups of weakly similar properties.. Uniprot accession numbers: Q5XJ10 for Gapdh and Q5MJ86 for Gapdhs.

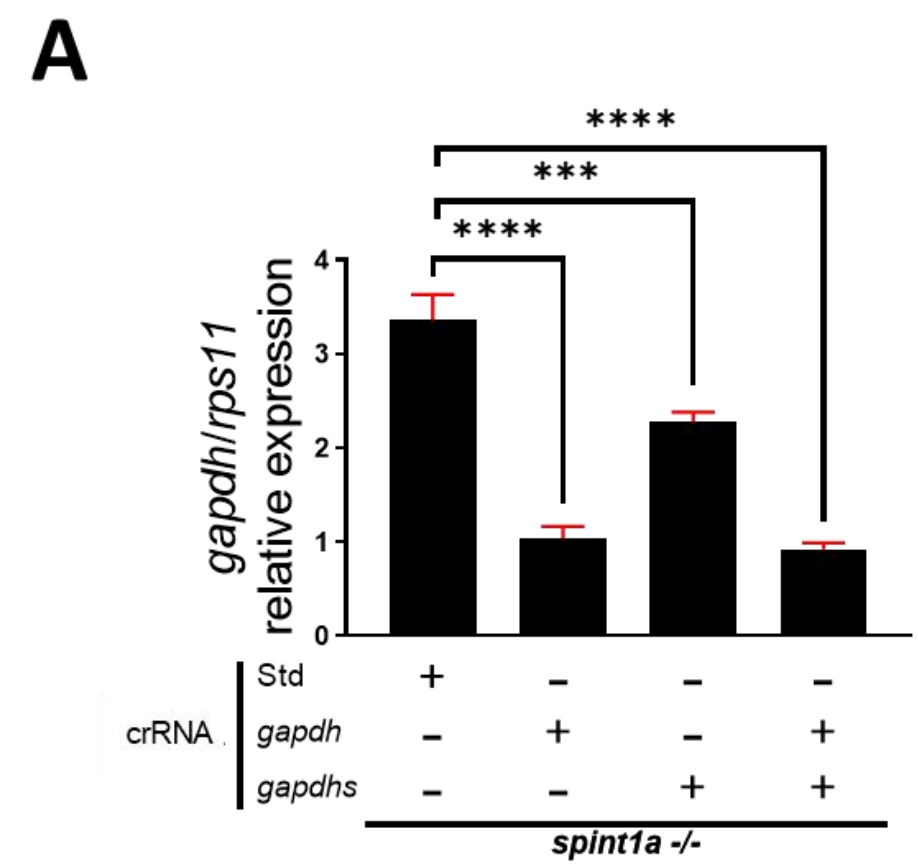


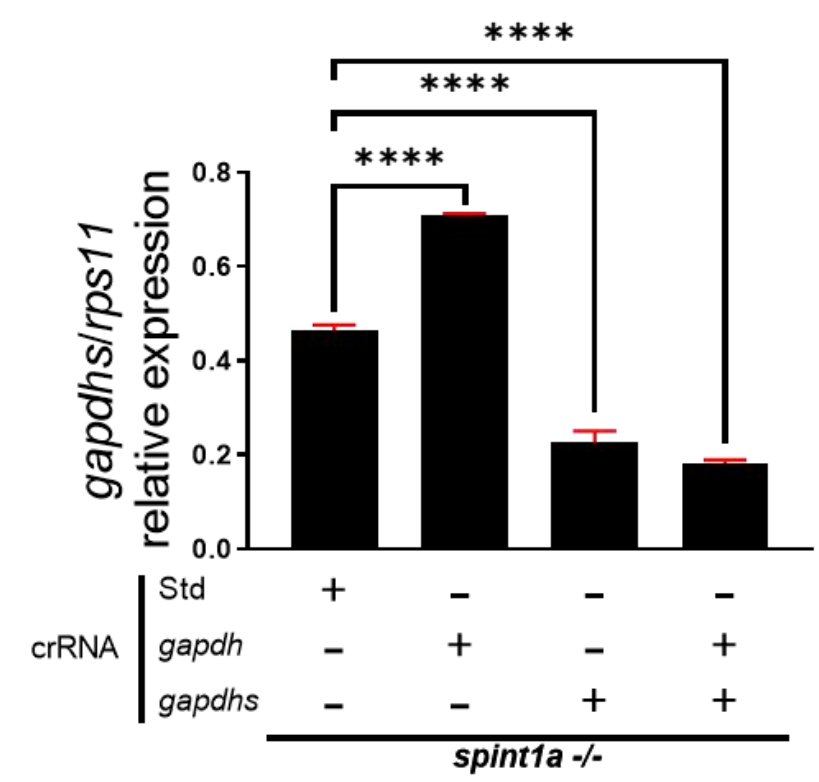


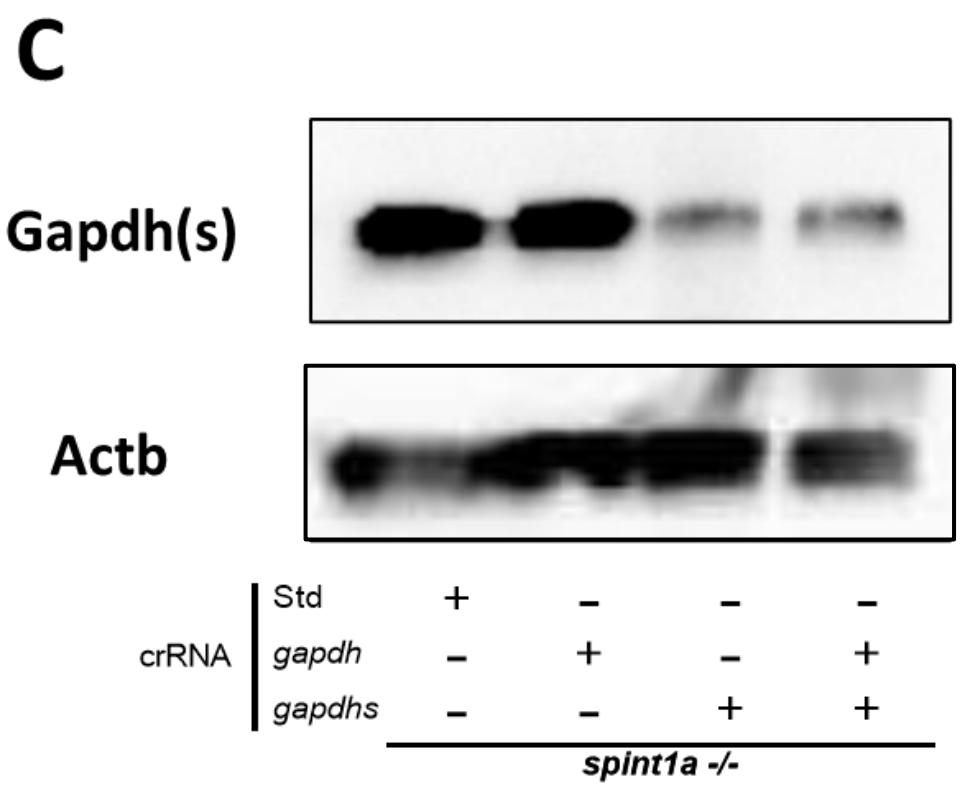


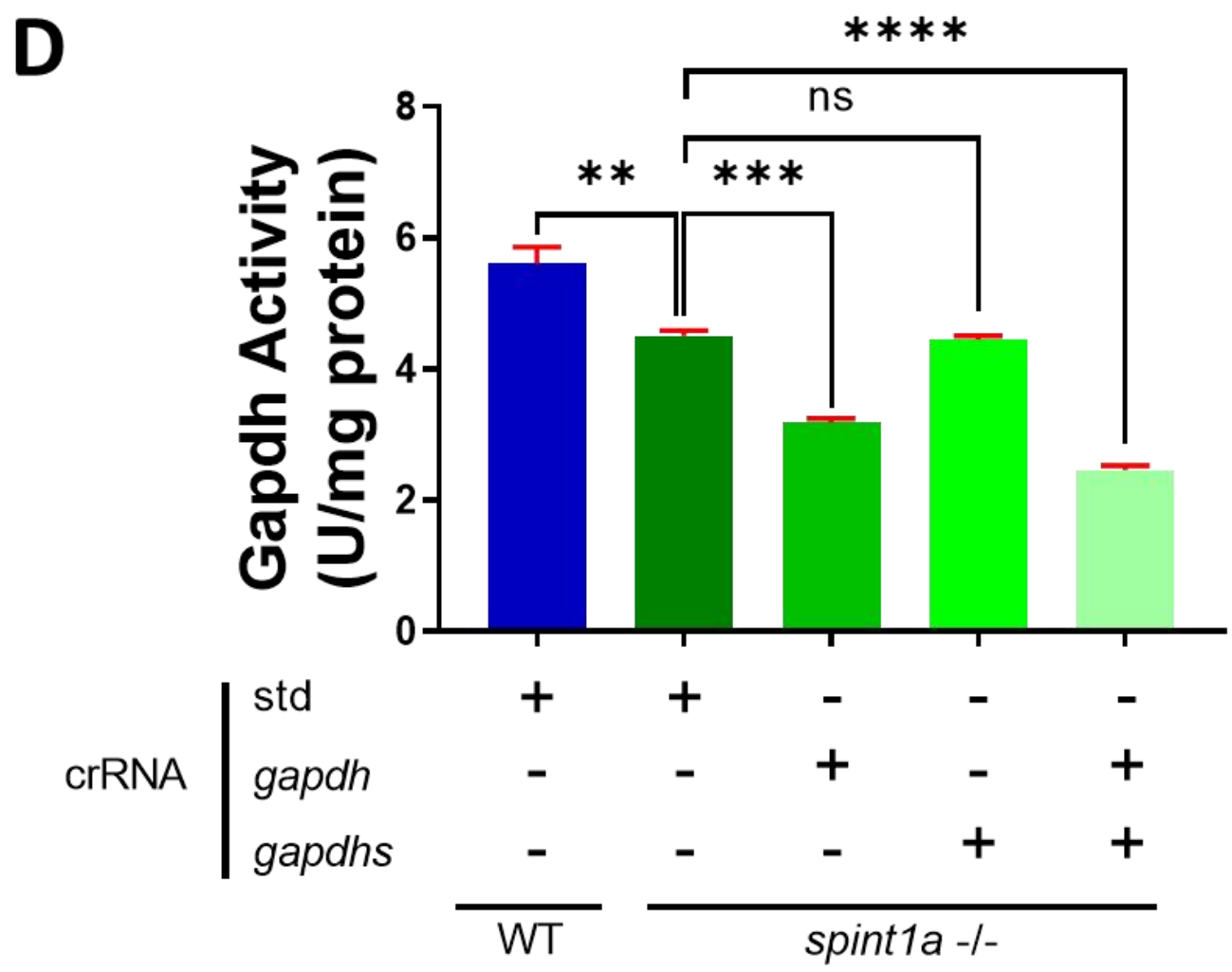


**Figure S7. Genetic inhibition of *gapdhs*, but not of *gapdh*, results in reduced protein amount and enzymatic activity of Gapdh. (A, B)** Transcript levels of *gapdh* (A) and *gapdhs* (B) after genetic inhibition of *gapdh* and/or *gapdhs*, assayed by RT-qPCR in 3 dpf Spint1a-deficient larvae. **(C)** Representative Western blot of Gapdh and Gapdhs protein amount in 3 dpf Spint1a-deficient larvae after genetic inhibition of *gapdh* and/or *gapdhs*. **(D)** Gapdh enzymatic activity in 3 dpf wild type and Spint1a-deficient larvae. Results are shown as the mean ± SD for each group. p-Values were calculated using 1-way ANOVA and Tukey multiple range test. **p≤0.01; ***p≤0.001; ****p ≤ 0.0001. DMSO, dimethyl sulfoxide; std, standard; crRNA, CRISPR RNA; WT, wild type; *gapdh*, glyceraldehyde-3-phosphate dehydrogenase; *gapdhs*, glyceraldehyde-3-phosphate dehydrogenese, spermatogenic; OD, Optical Density; U, Enzymatic activity units.

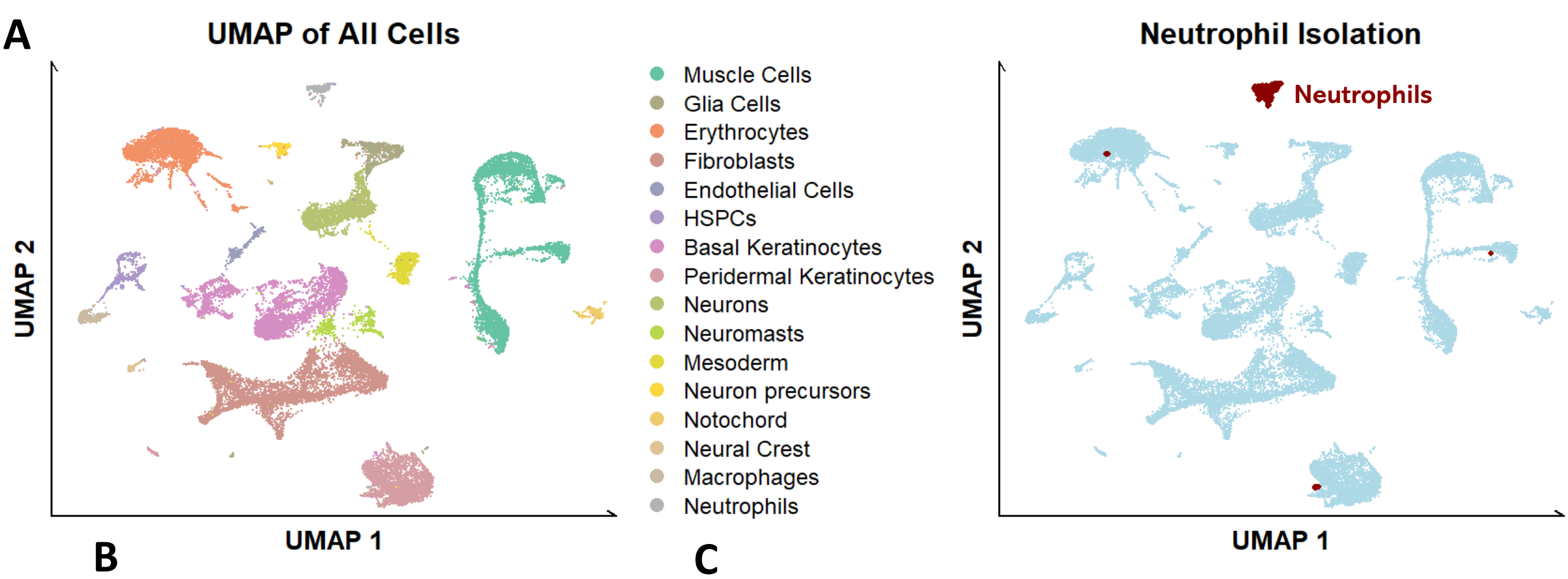


**Figure S8. Neutrophil reclustering reveals eight different neutrophil subclusters. (A)** Neutrophil population (highlighted in red) was selected based on the expression of the markers *mpx* and *lyz*, and they were then reclustered. **(B, C)** The reclustering generated eight different clusters, numbered from 0 to 7. UMAP shows neutrophils grouped by clusters (B) and sample origin (C). **(D)** Bar chart shows cluster organization, indicating the percentage of cells from each sample that constitute each cluster. WT, wild type; UMAP, Uniform Manifold Approximation and Projection for Dimension Reduction.

**A**

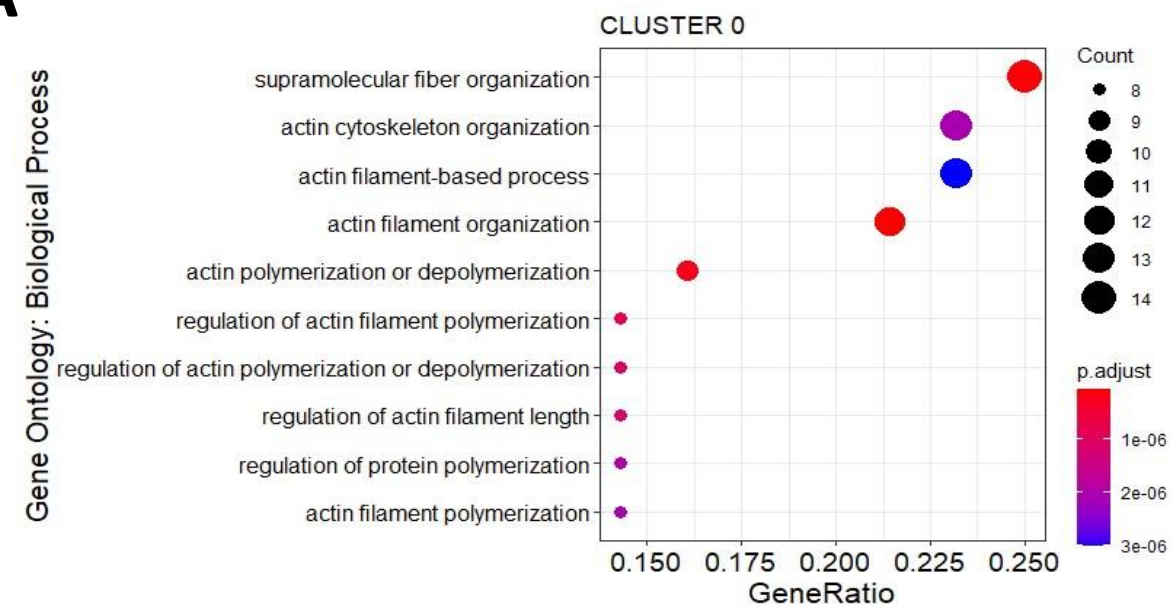


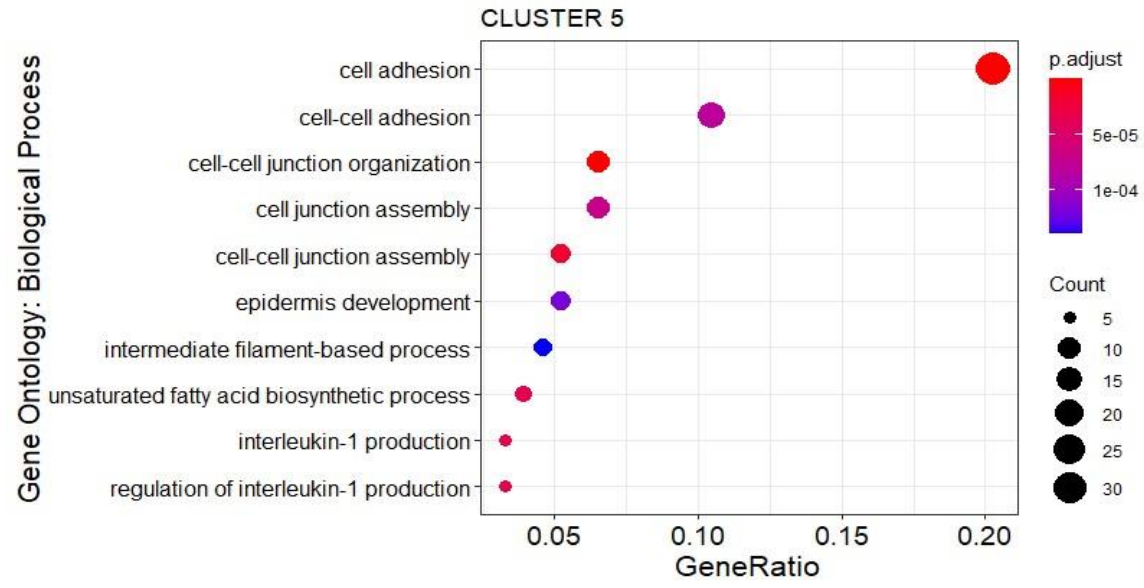


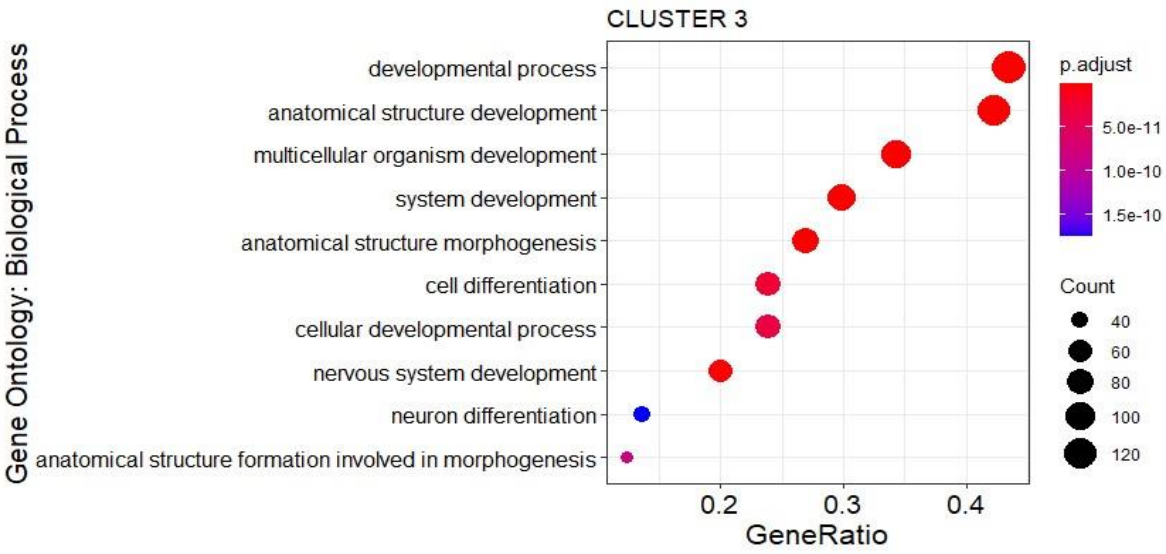


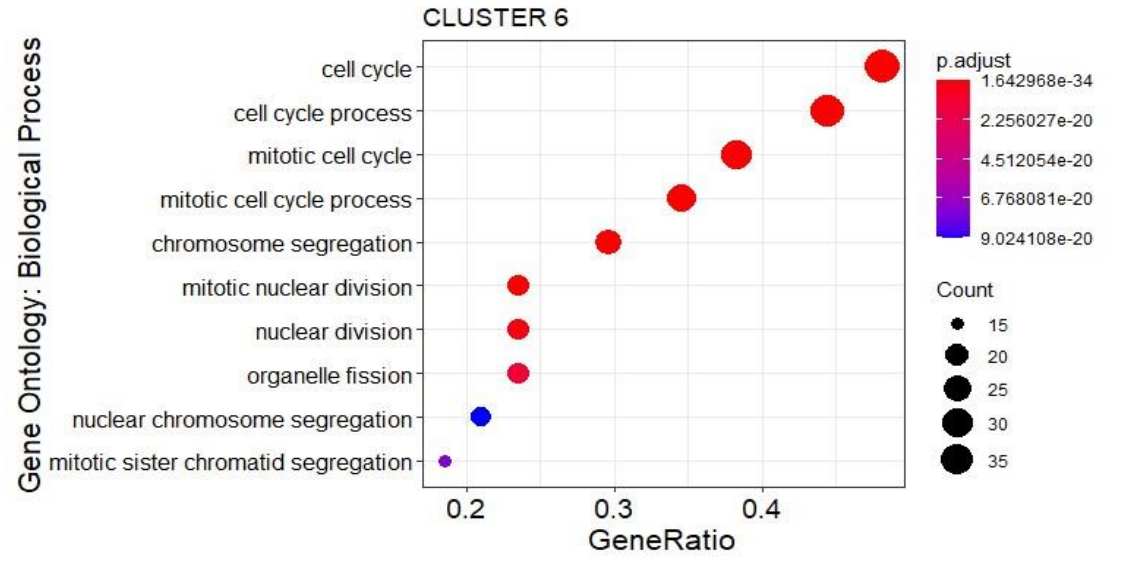


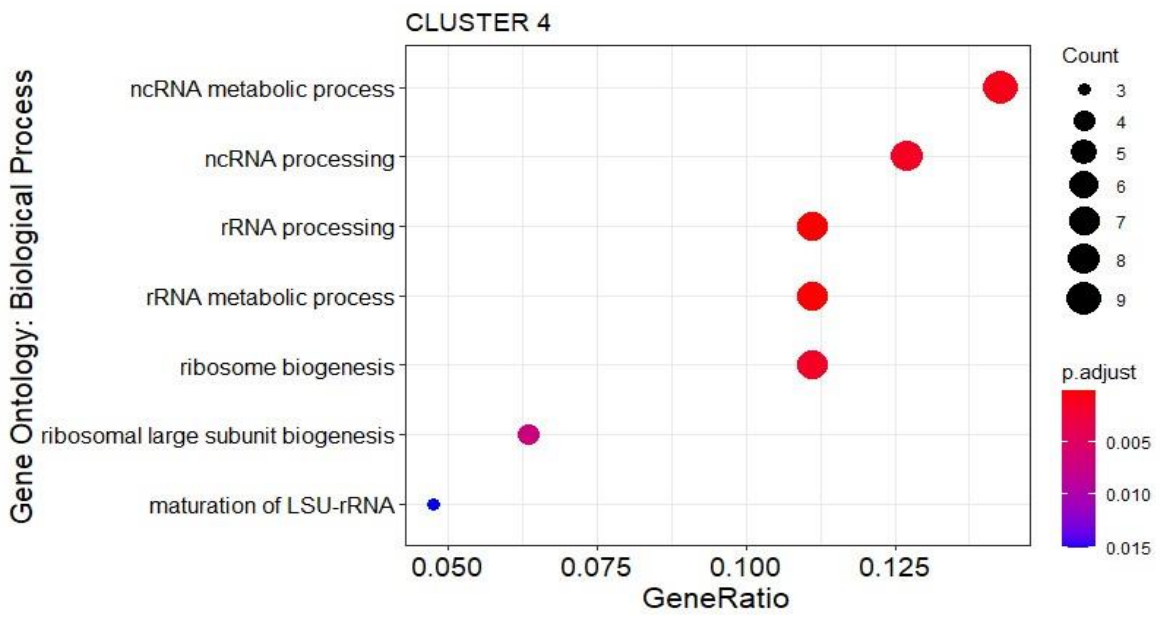


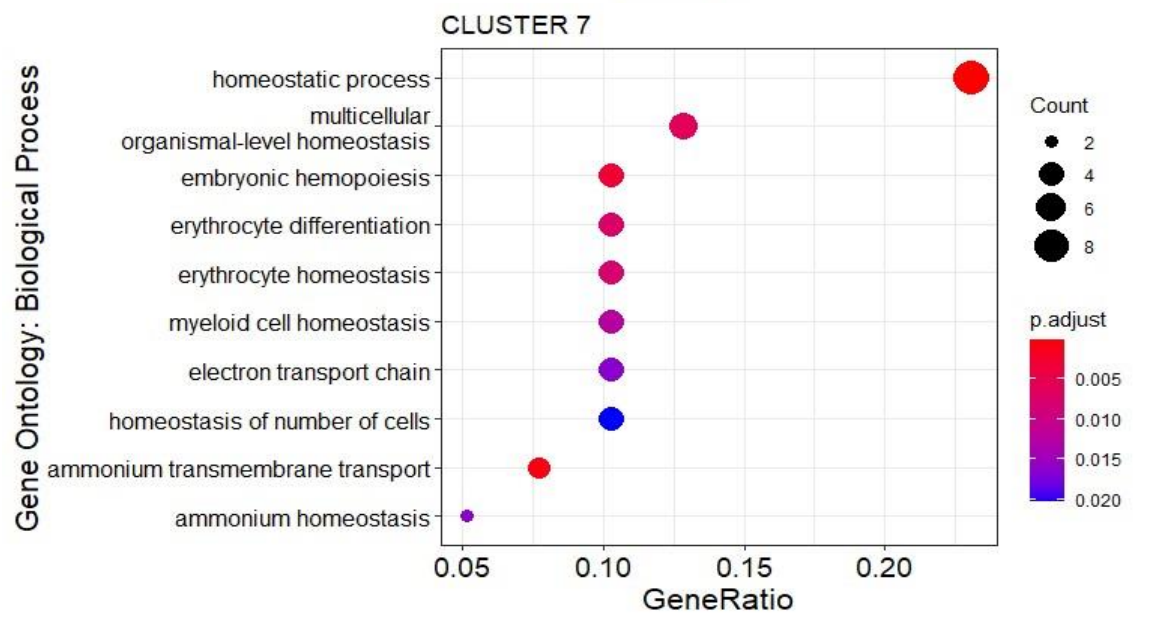


**B**

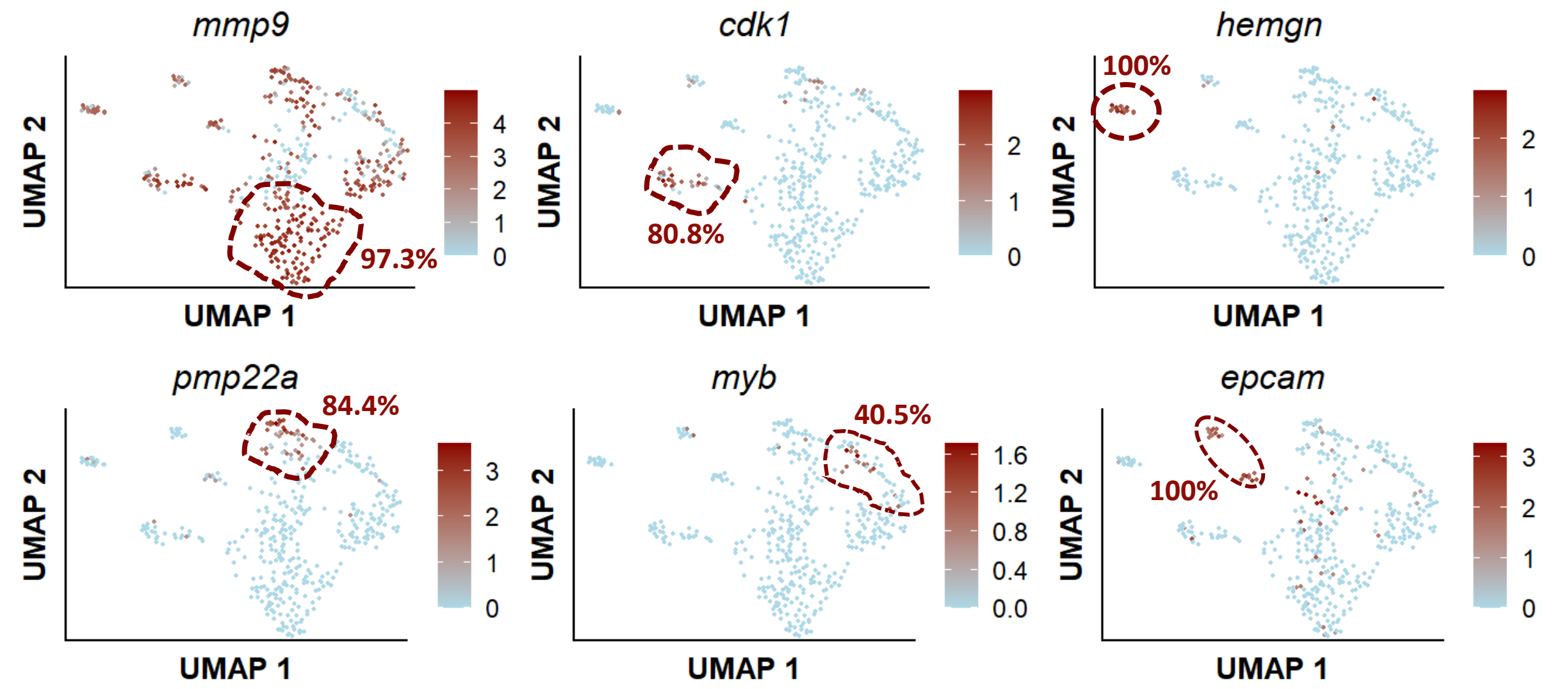


**Figure S9. Characterization of neutrophil subclusters obtained by scRNA-seq analysis. (A)** Dotplots showing the 10 most significantly altered Gene Ontology: Biological Process pathways in the neutrophil subclusters 0, 3, 4, 5, 6 and 7. No significant pathways were obtained for clusters 1 and 2. **(B)** FeaturePlot showing the most differentially expressed gene of each neutrophil subcluster and their relative abundance. *mmp9,* matrix metalloproteinase 9*; pmp22a,* peripheral myelin protein 22a*; myb,* v-myb avian myeloblastosis viral oncogene homolog*; epcam,* epithelial cell adhesion molecule*; cdk1,* cyclin dependent kinase 1*;*

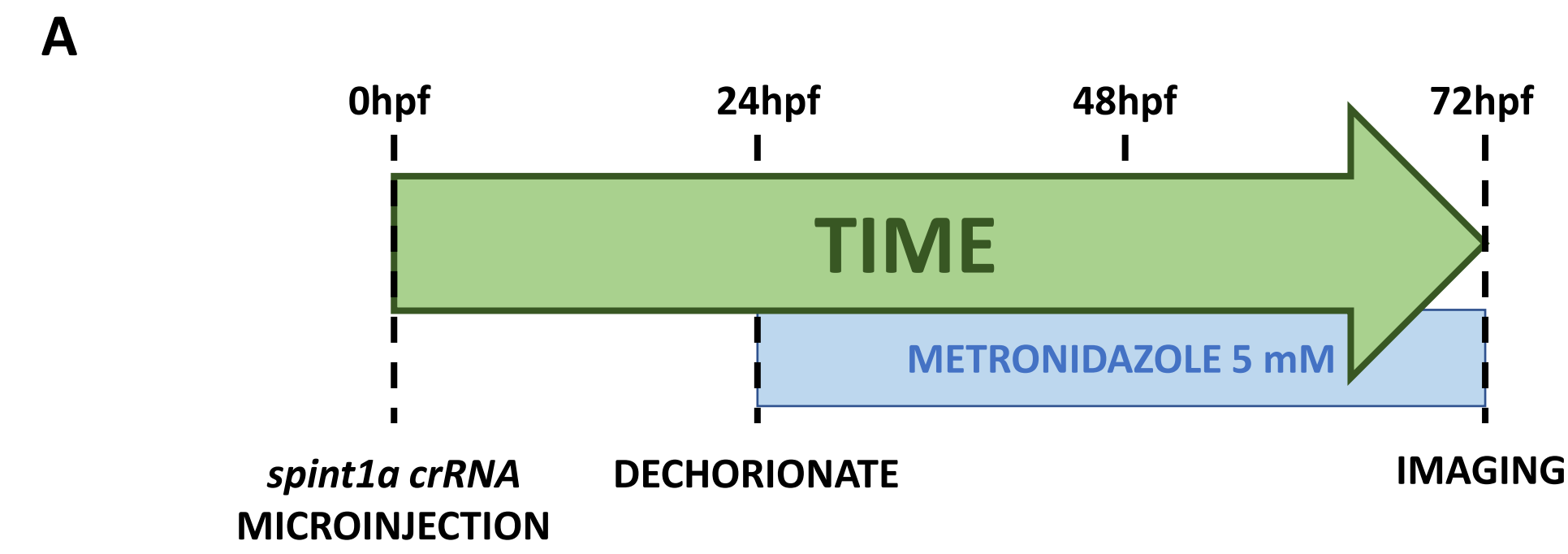


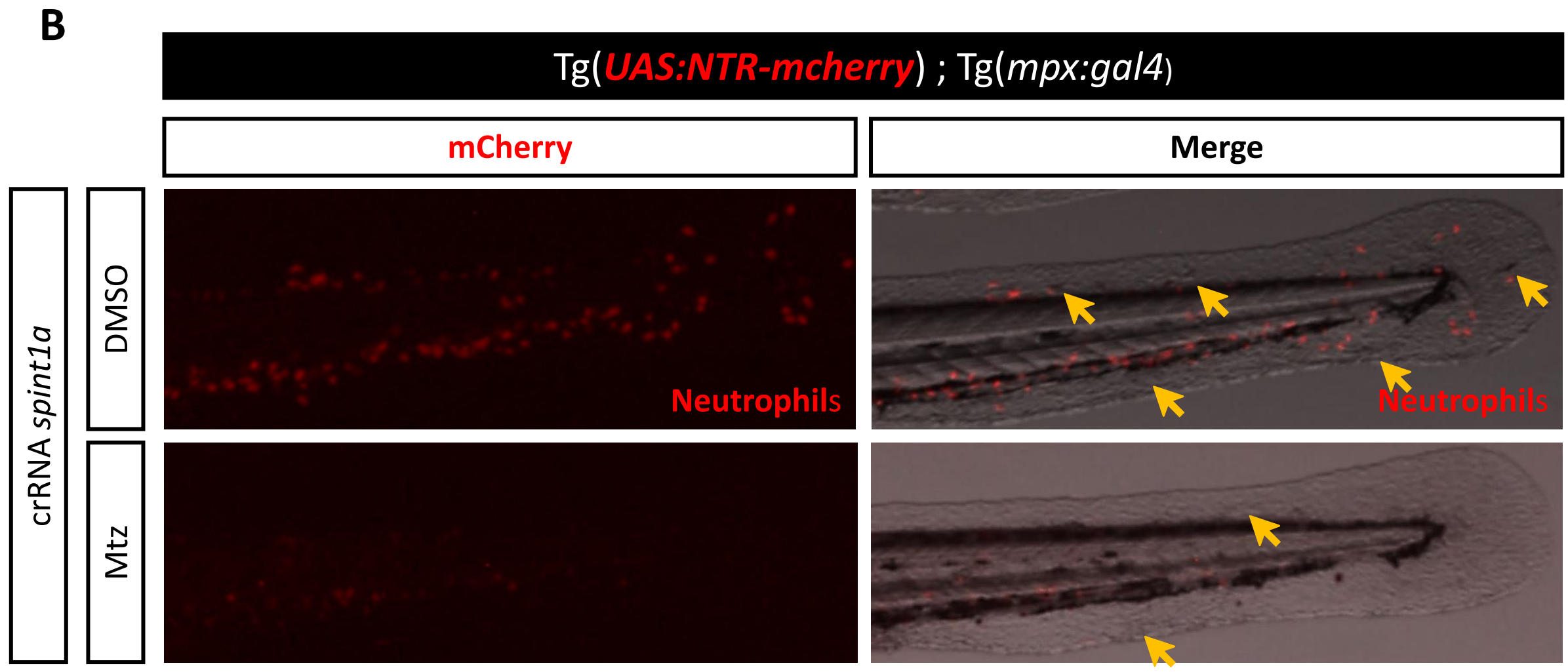


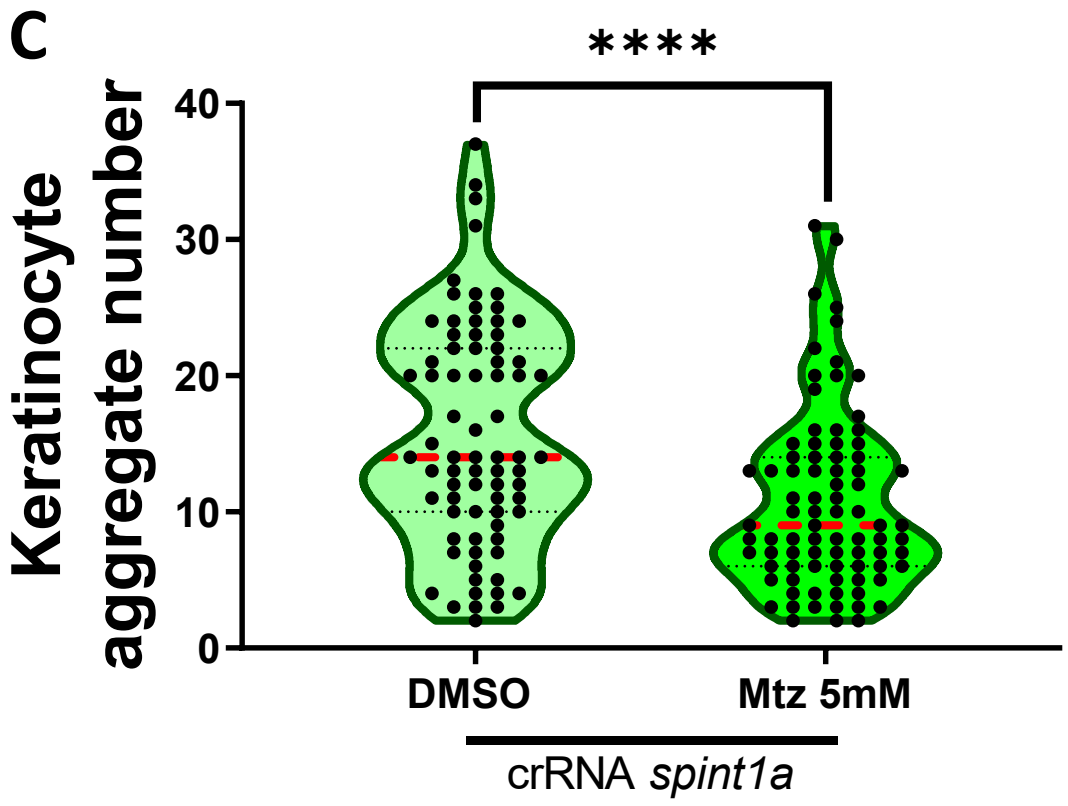


**Figure S10. Neutrophil ablation alleviates chronic skin inflammation. (A)** The lines *TgBAC(mpx:GAL4-VP16*) and *Tg(UAS-E1B:NTR-mCherry)* were crossed and the embryos were microinjected with *spint1a* crRNA/Cas9 complexes at one-cell state of development. At 1dpf embryos were dechorionated and treated with either DMSO or 5 mM metronidazole (MTZ) for 48 h. Three dpf larvae were imaged and the phenotype was quantified. **(B, C)** Keratinocyte aggregate number (B) and representative merge images showing skin and neutrophils (C). Yellow arrows label keratinocyte aggregates in the skin. Each dot represents one individual, and the median for each group is also shown. p-Values were calculated using Student's *t* test. ****p ≤ 0.0001. DMSO, dimethyl sulfoxide; std, standard; crRNA, CRISPR RNA; Mtz, metronidazole.

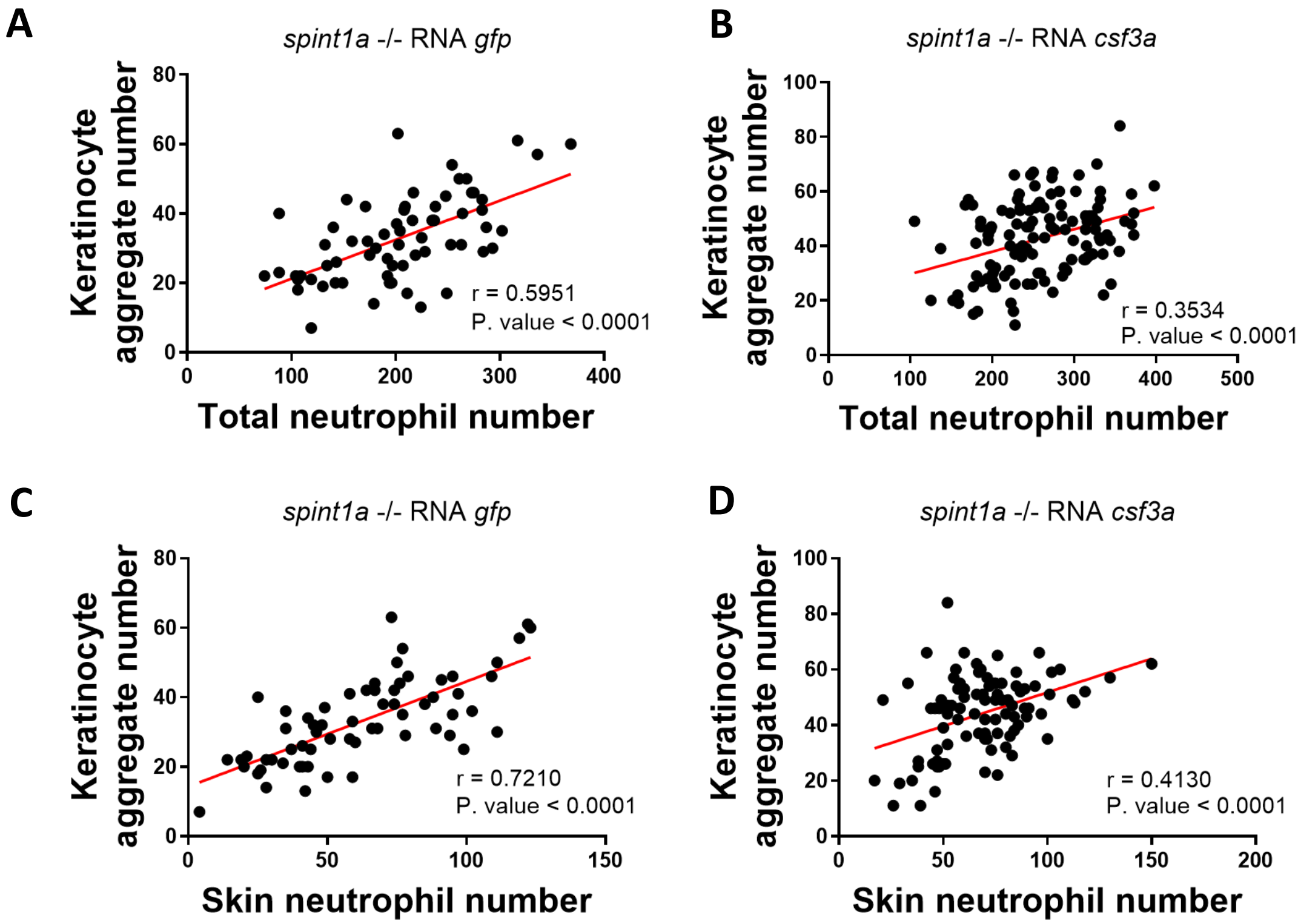


**Figure S11. Csf3a-driven neutrophilia exacerbates chronic skin inflammation.**. Correlation between the number of keratinocyte aggregates and the number of neutrophils (A, B) and between the number of neutrophils infiltrated in the skin and the number of keratinocyte aggregates (C, D) in Spint1a-deficient larvae microinjected with the mRNA of *gfp* (A, C) or *csf3a* (B, D). Each dot represents one individual whose number of neutrophils (total or in the skin) and number of aggregates was quantified. p-Values were calculated using Pearson correlation. *gfp*, green fluorescent protein; *csf3a*, colony stimulating factor 3a.

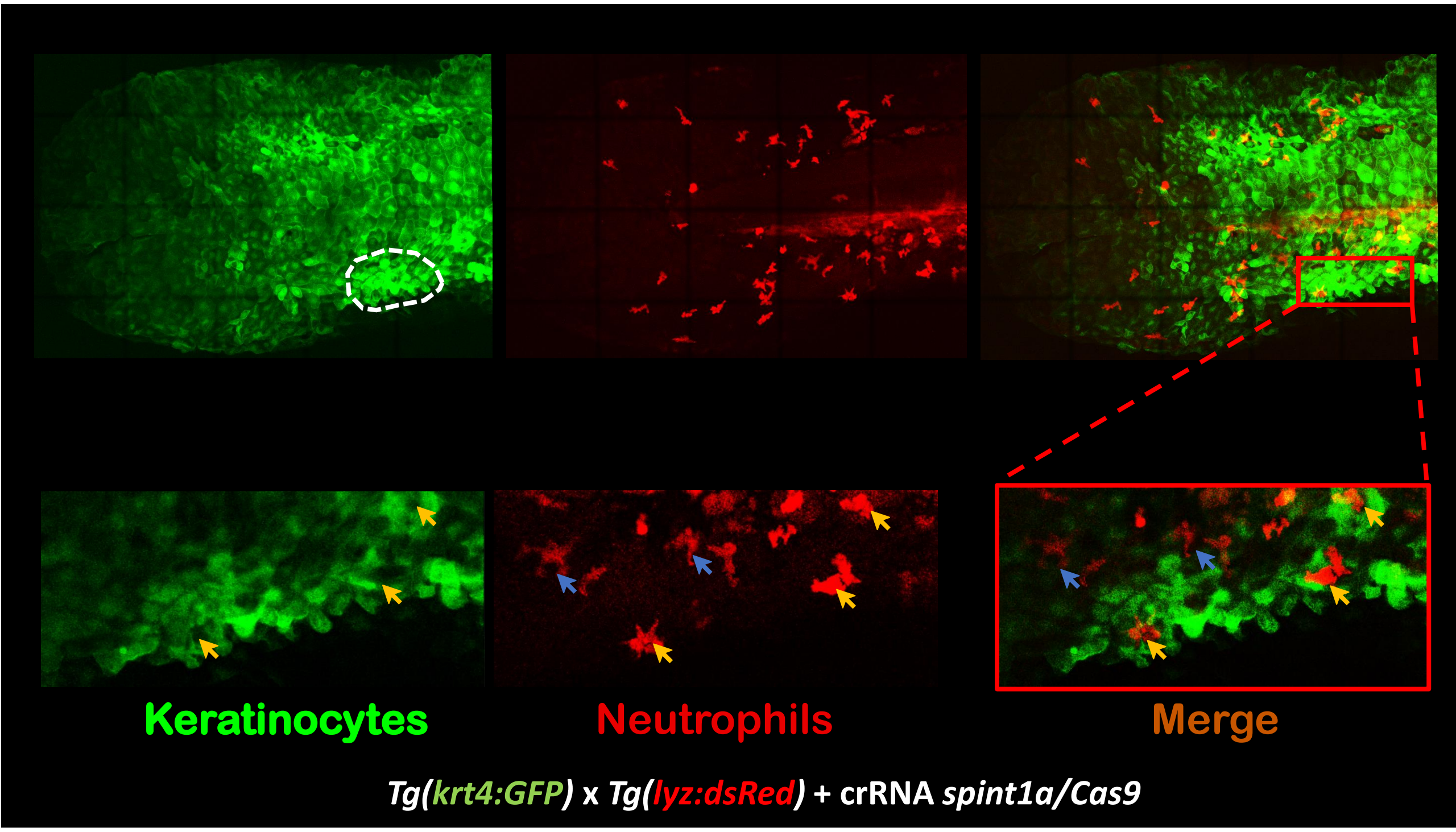


**Figure S12. Neutrophil and keratinocyte interaction in the inflamed skin of the Spint1a-deficient larvae.** Representative confocal microscopy images from Tg(*krt4:GFP; lyz:dsRED*) larvae of 3 dpf microinjected with *spint1a* crRNA/Cas9 complexes at the one-cell stage. Neutrophils interacting with the keratinocyte of a selected aggregate (dotted line) are indicated with yellow arrows, while the non-interacting neutrophils are indicated with blue arrows. *Krt4, keratin 4*; crRNA, CRISPR RNA; *lyz, lysozyme*.

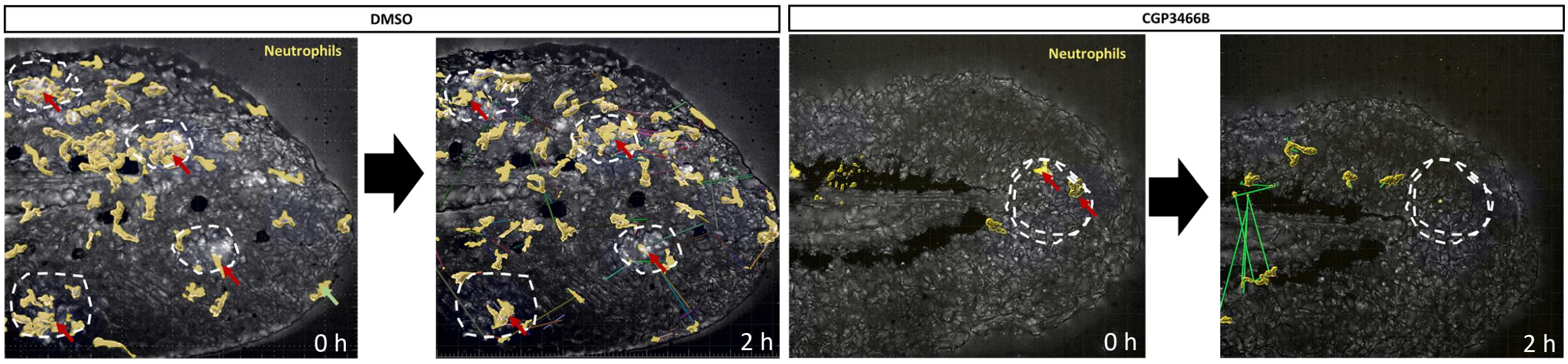


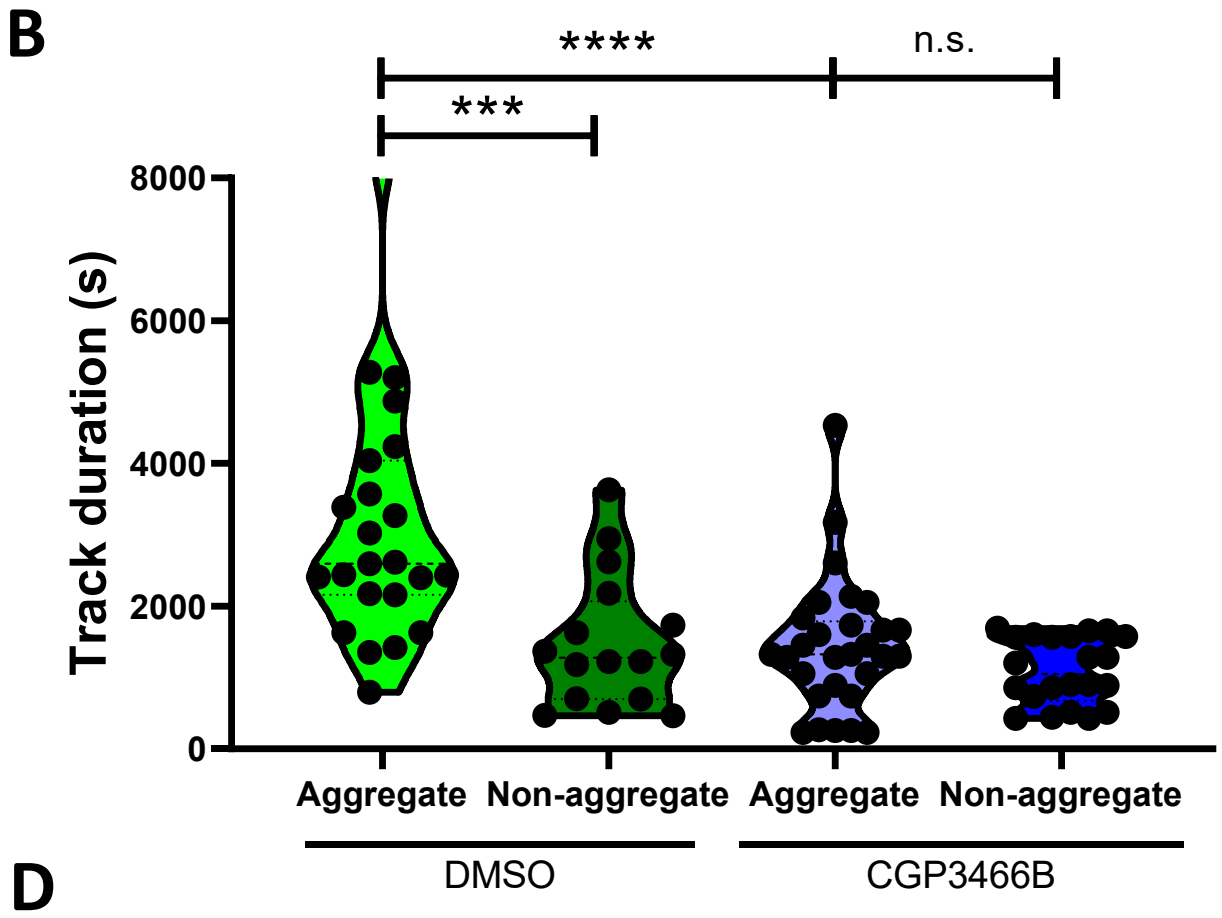


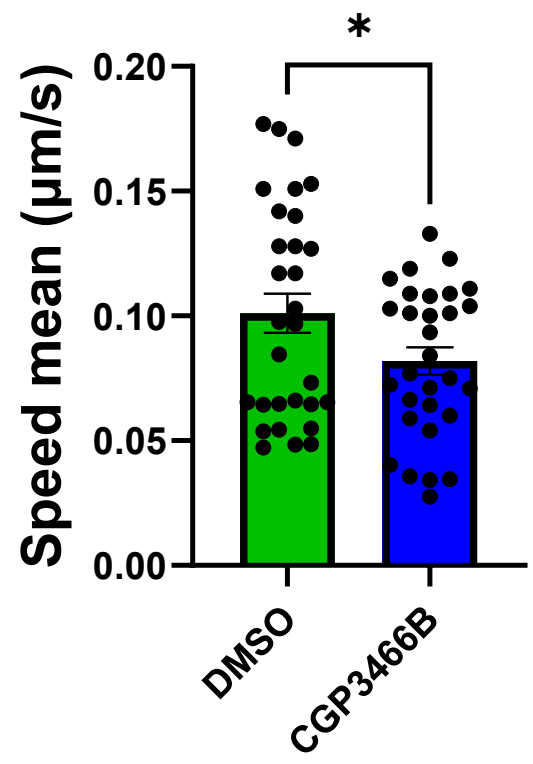


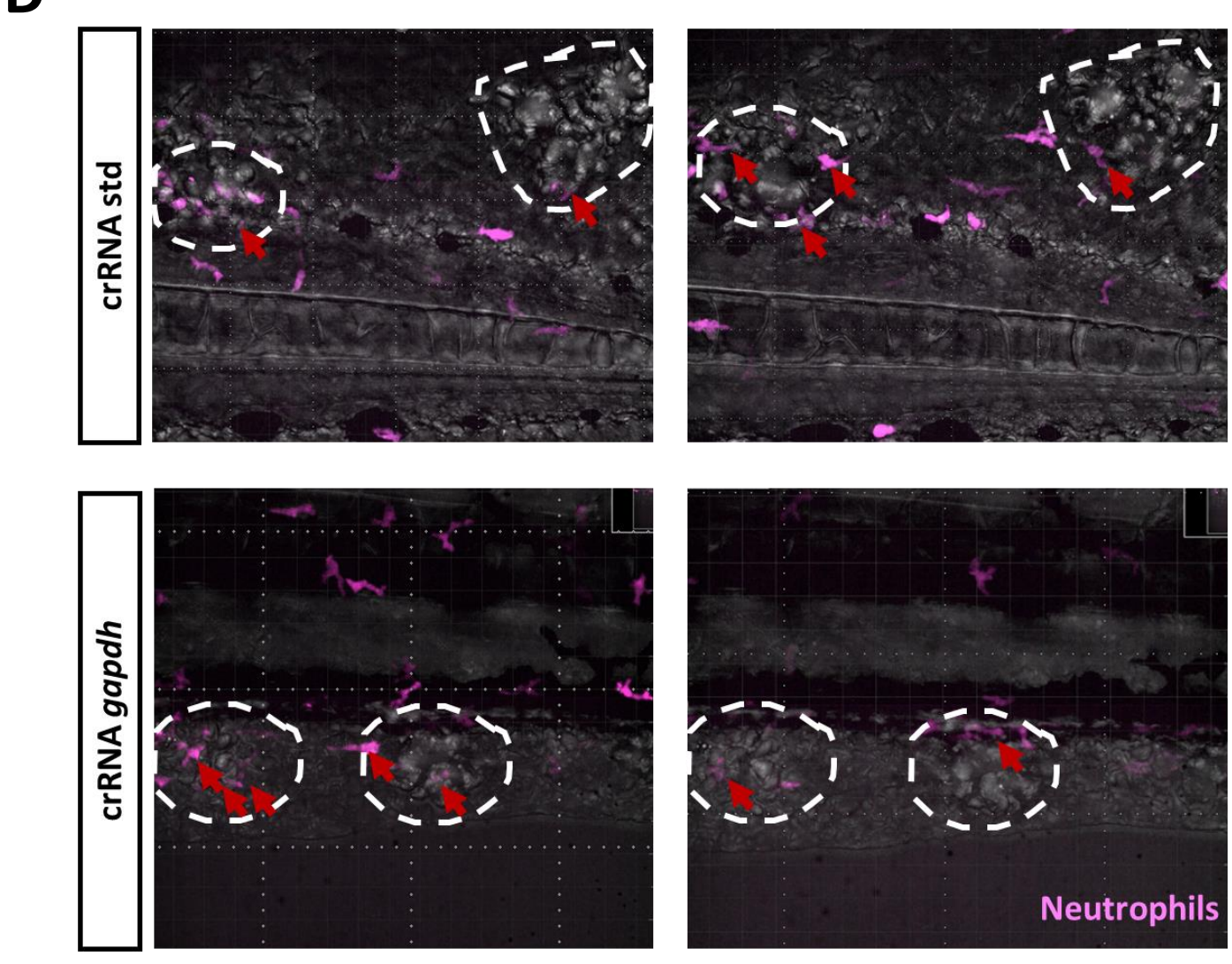


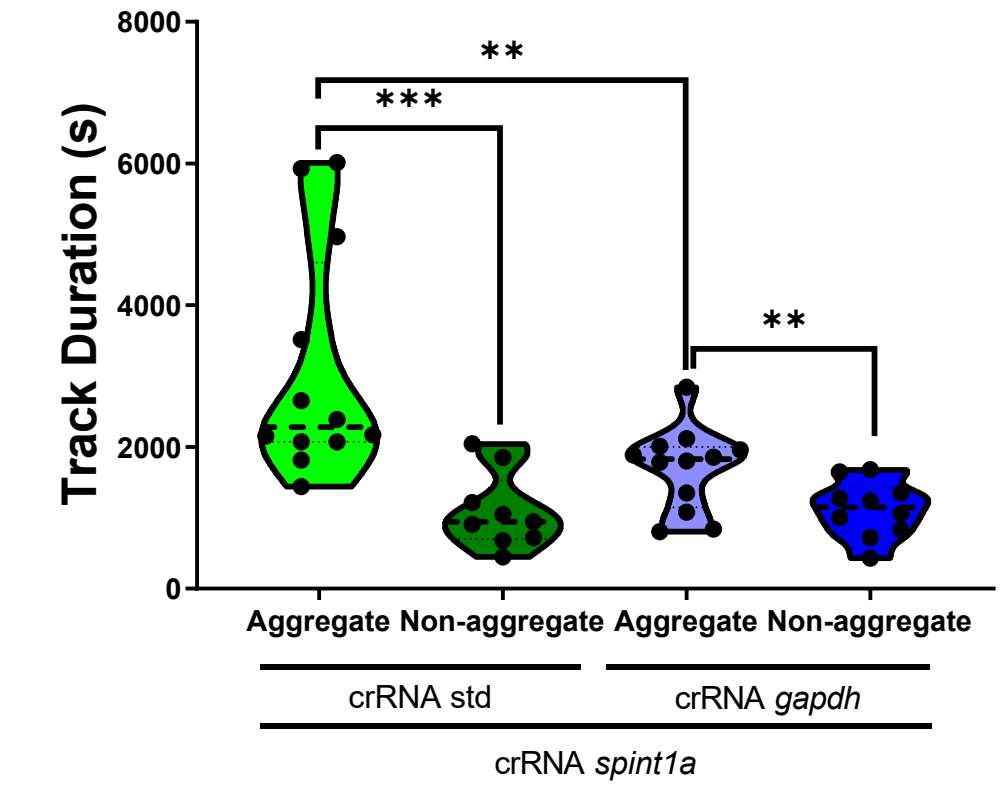


**Figure S13. Inhibition of Gapdh nuclear translocation reduces neutrophil-keratinocyte interactions in the inflamed skin of Spint1a-deficient larvae.** *Tg(lyz:BFP)* larvae were treated with either DMSO or CGP3466B from 48 to 72 hpf **(A-C)** or microinjected with standard (std) or *spint1a* crRNA/Cas9 complexes **(D, E)** and recorded for 4h at 72 hpf using a spinning disk confocal microscope. **(A, D)** Representative merge images of long-term movies of skin larvae. Left images were taken at 0 h and right images at 2 h. The keratinocyte aggregate areas are depicted with a white dotted line, while red arrows label the neutrophils interacting with them. The neutrophils are colored in yellow with their tracks represented in dragon tail format. **(B, E)** Mean time each neutrophil interacts with keratinocyte aggregates. **(C)** Mean speed of each neutrophil. Each dot represents the mean of all the neutrophils of one individual during the 4 h of the movie, and the median (B, E) or mean ± SD (C) for each group is also shown. p-Values were calculated using 1-way ANOVA followed by Tukey multiple range test (C, D, F) and Student's *t* test (D). n.s., non-significant; *p ≤ 0.05; **p ≤ 0.01; ***p ≤ 0.001; ****p ≤ 0.0001. ANOVA, analysis of variance; *lyz*, lysozyme; DMSO, dimethyl sulfoxide.

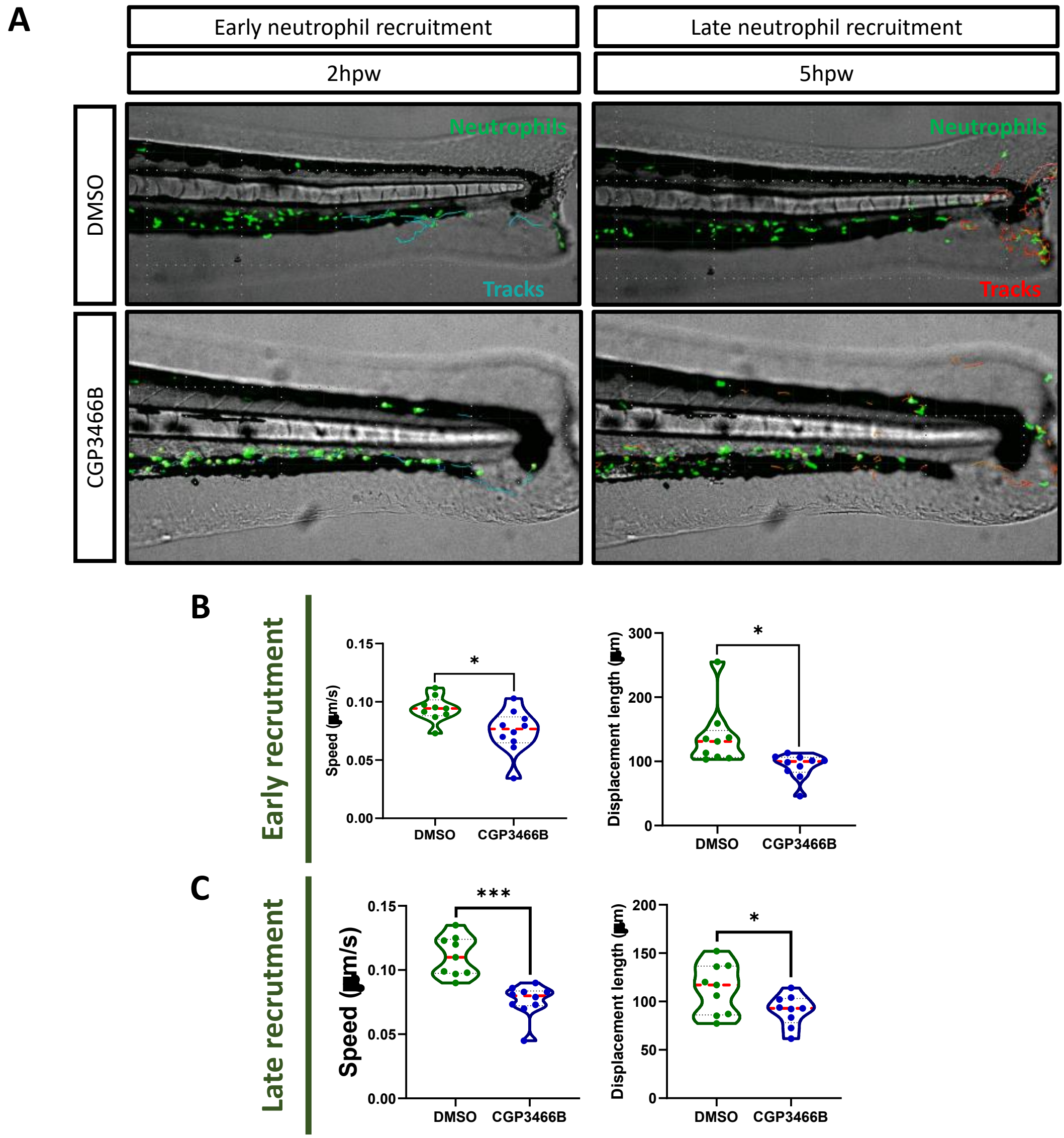


**Figure S14. Impact of pharmacological inhibition of Gapdh nuclear translocation in the early and late neutrophil recruitment to tail wounding. (A)** Representative merge images shown the tails, the neutrophils and their tracks in dragon tail format of DMSO- and 10 µM CGP3466B-treated larvae at 2 hpw (end of the early recruitment phase) and at 5 hpw (end of late recruitment phase). **(B, C)** Speed and displacement length during early (B) and late (C) neutrophil recruitment phases. Each dot represents one individual, and the median for each group is also shown. p-Values were calculated using Student's *t* test. *p ≤ 0.05, ***p ≤ 0.001. Hpw, h post-wounding; DMSO, dimethyl sulfoxide.

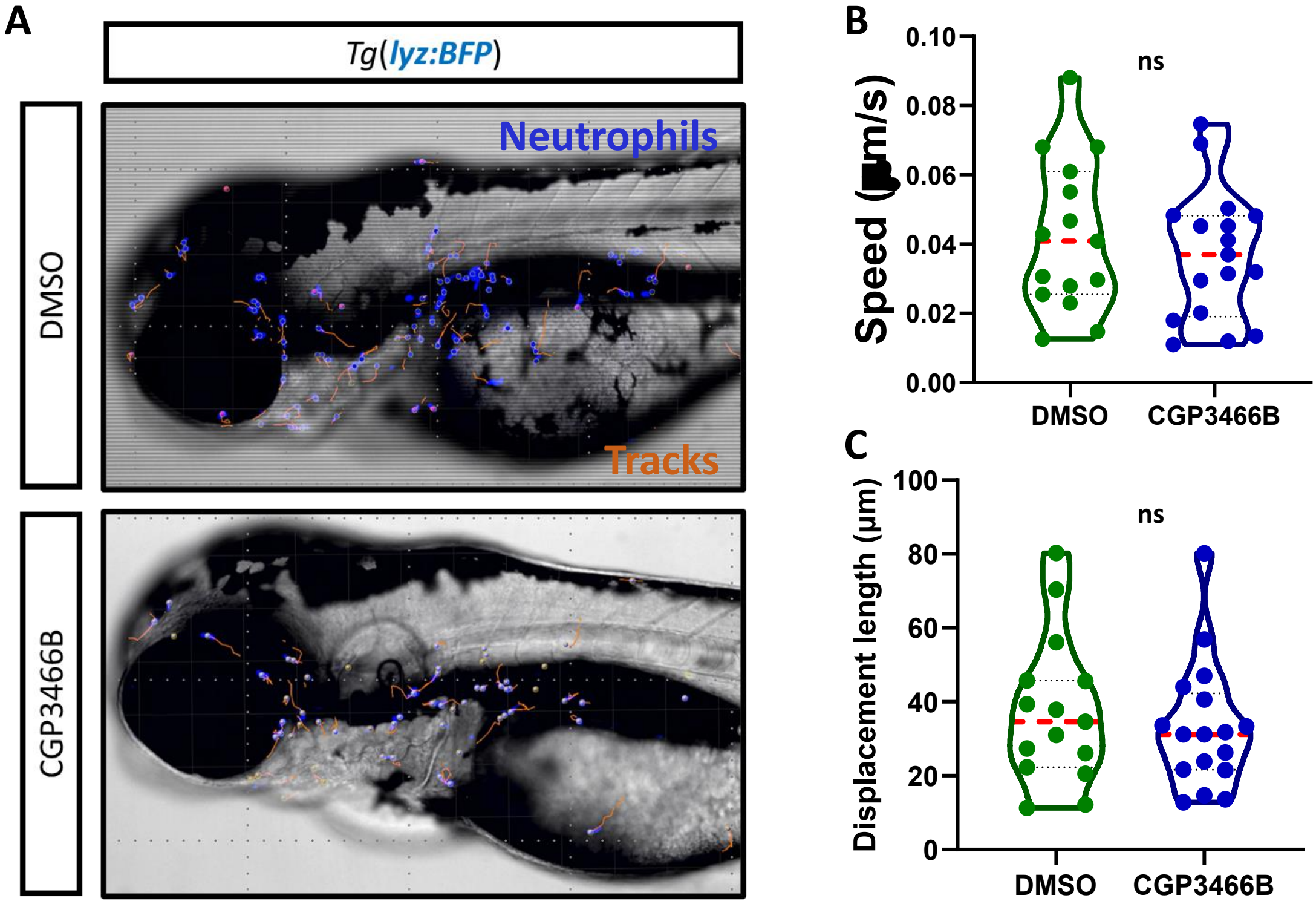


**Figure S15. Random neutrophil migration is unaffected by Gapdh nuclear translocation. (A)** Representative images of the heads, the neutrophils and their tracks in dragon tail format of DMSO- and 10 µM CGP3466B-treated 3dpf larvae. **(B, C)** Speed **(B)** and displacement length **(C)**. Each dot represents one individual, and the median for each group is also shown. p-Values were calculated using Student's *t* test. ns, non-signficant. Hpw, hours post wound; DMSO, dimethyl sulfoxide.

**A**

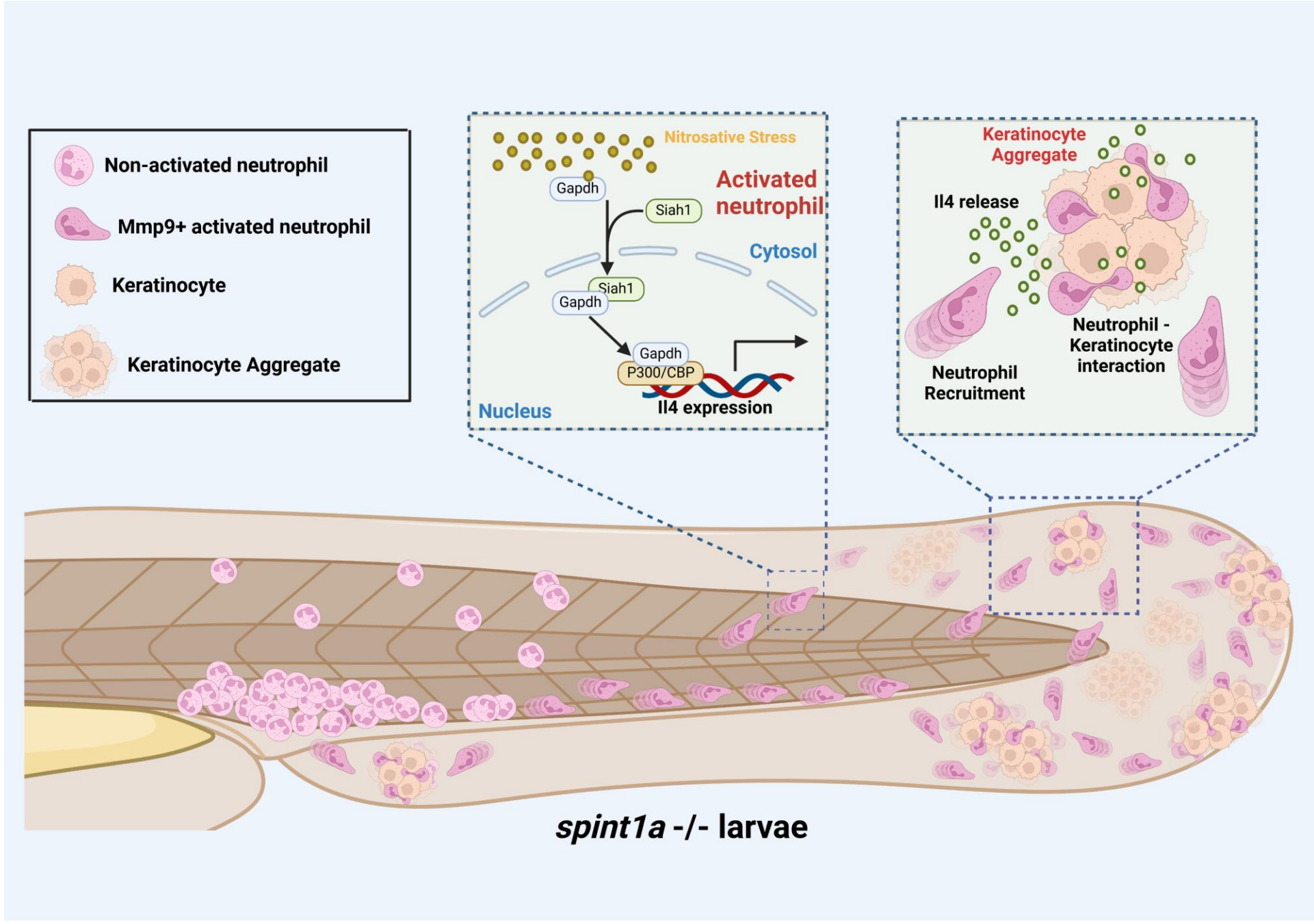


**B**

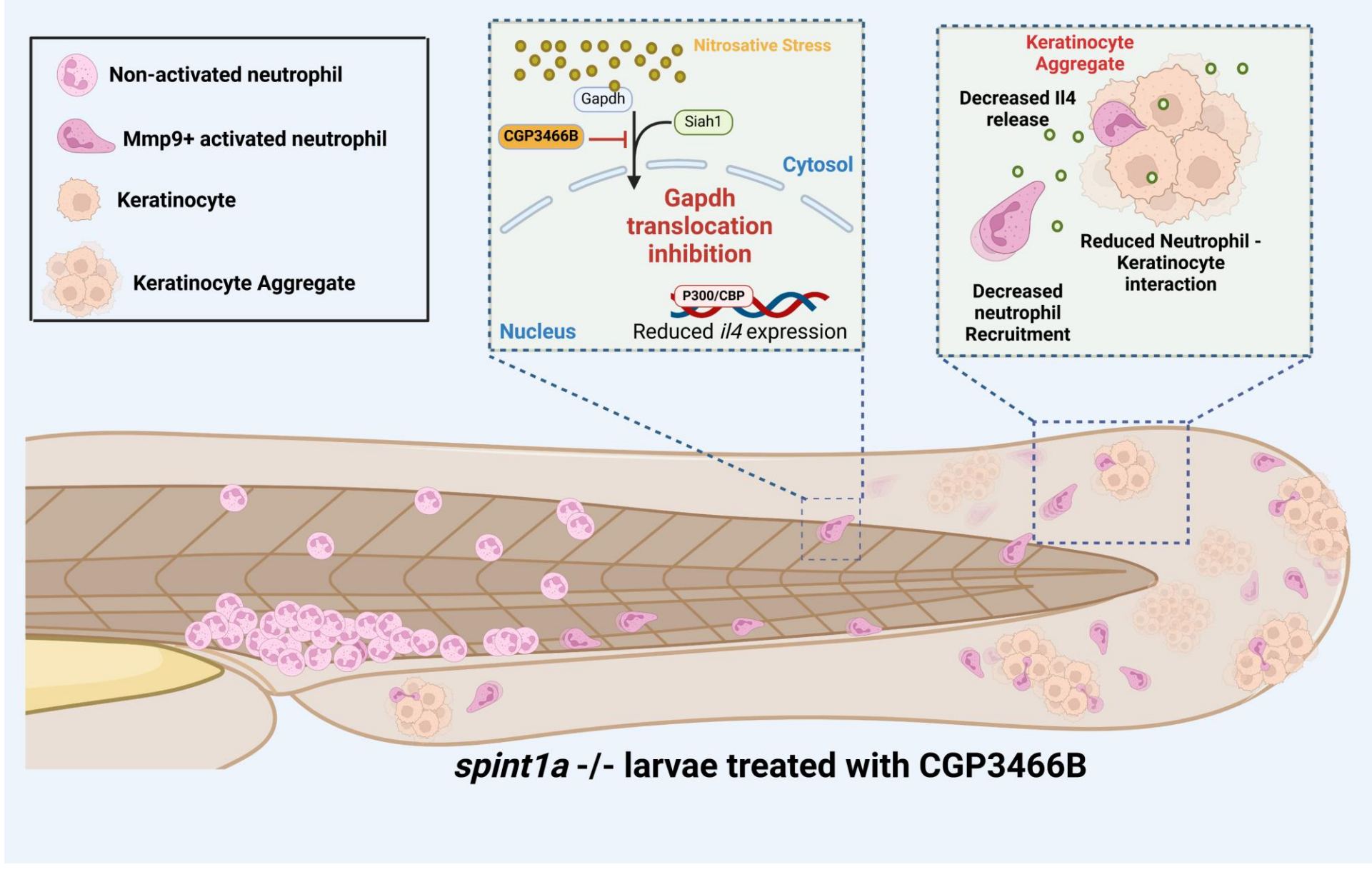


**Figure S16. GAPDH nuclear translocation regulates neutrophil behavior during inflammation. (A)** GAPDH nuclear translocation modulates the expression of genes such as *il4*, promoting neutrophil recruitment to keratinocyte aggregates in the skin, increasing their speed and displacement length. Once in the aggregates, neutrophils interact with keratinocytes for extended periods, likely releasing Il4, which exacerbates inflammation. **(B)** Inhibition of GAPDH nuclear translocation reduces neutrophil recruitment to the skin, their speed and displacement length, the duration of neutrophil-keratinocyte interactions, and Il4 release. Consequently, more neutrophils remain retained in the caudal hematopoietic tissue, leading to reduced inflammation. (Created with BioRender).